Physics – Uspekhi **67** (3) 272 – 291 (2024)

REVIEWS OF TOPICAL PROBLEMS PACS numbers: 07.85.Qe, **75.25. – j, 76.80. + y**

Coherent nuclear fluorescence: synchrotron Mössbauer radiation

G V Smirnov

DOI: https://doi.org/10.3367/UFNe.2023.09.039569

Contents

Abstract. Purely nuclear diffraction of synchrotron radiation enables the glow of excited atomic nuclei to be observed in the absence of background nonresonant electron scattering. Nuclei excited in an iron borate crystal can generate in the crystal directed gamma radiation with a narrow spectral band. Based on the remarkable properties of iron borate, the first source of synchrotron Mössbauer (SM) radiation was created a quarter of a century ago. The history of the emergence and development of a new branch of optics — quantum optics of resonant gamma radiation — is briefly reviewed, the physical concepts underlying operation of the SM radiation source are presented, and the design of such a source deployed in the optical line of the European Synchrotron Center (ESRF) is described. Options for using SM radiation in the physics of the condensed state of matter, quantum optics, geophysics, planetology, and other areas of research are presented.

Keywords: purely nuclear diffraction, synchrotron Mössbauer radiation

1. Introduction

Coherence is one of the fundamental characteristics of oscillatory and wave processes. Radiative transitions in nuclear isomers are a remarkable example of the persistence of coherence in nature. The experimentally observed exponential behavior of nuclear de-excitation reveals the harmonic nature of oscillations of the transition current between the excited and ground states of the nucleus, to the ground state, in which a strict phase correlation is maintained. The extremely long duration of the isomeric transition process attests to the fact that phase correlation can persist for a very long time. A striking example is the transition from the first excited state of the ^{67}Zn nucleus to the ground state. During the characteristic time of this transition, $\sim 10^{-5}$ s, about 10^{15} correlated oscillations of the nuclear current occur, which is an amazing manifestation of the temporal coherence of the oscillatory process in nature!

So, by measuring the time dependence of the de-excitation of a nuclear isomer, we obtain evidence that coherence exists in intranuclear transition processes. However, thermal vibrations of atoms, leading to frequency modulation of the emitted radiation, prevent the latter from inheriting the natural properties of coherence of intranuclear currents and, in particular, hinder the observation of the natural width of the spectral line, comparable to the width of the nuclear isomeric level. A remarkable feature of the Mössbauer effect [1] is that gamma radiation emitted by a bound nucleus can preserve and maintain the property of coherence of intranuclear currents. Mössbauer's discovery makes it possible, using the example of nuclear resonance scattering, to verify the coherence of resonant fluorescence, studied theoretically in the 1930s by Heitler [2]. The recoilless emission and absorption of gamma quanta by bound nuclei enable elastic scattering of gamma radiation in crystals to be realized. In elastic nuclear resonance scattering, the absorption and emission of a quantum cannot be considered as two independent scattering events, an assertion which is true even when the lifetime of the isomeric state is enormous on nuclear scales. In this case, nuclear resonance fluorescence is a single-quantum process in which the scattered radiation is coherent with the incident radiation.

It is known, however, that resonant fluorescence in the case of nuclear isomers makes only a minor contribution to quantum scattering on a nucleus. This is due to the over-

G V Smirnov
National Research Center Kurchatov Institute,
pl. Akademika Kurchatova 1, 123182 Moscow, Russian Federation
E-mail: g.smirnov37@mail.ru

Received 17 March 2023
Uspekhi Fizicheskikh Nauk **194** (3) 291 – 311 (2024)
Translated by M Zh Shmatikov

whelming dominance in this process of internal electron conversion, in which the excitation energy of the nucleus is transferred directly to the electrons of the atom. This may give the impression that the issue of coherence in nuclear resonance fluorescence can only be of academic interest. Fortunately, contrary to expectations, theoretical and experimental studies conducted in the 1960s–1980s yielded a different and much more optimistic picture. In addition to showing the persistence of coherence in nuclear resonance scattering, it was found that, under certain conditions, due to coherence, nuclear fluorescence can even become the dominant channel of interaction of gamma radiation with nuclei. We now focus on the most important moments in the history of this issue.

Shortly after the Mössbauer effect was discovered, interest in the issue of coherence of gamma radiation from isomeric nuclei increased noticeably. As early as 1960, Black and Moon [3] observed the interference of two processes of gamma ray scattering on an atom, significantly different in their physical nature: potential scattering on the electron shell of the atom and resonant scattering on the atomic nucleus. The very existence of interference of resonant scattering with an apparently coherent potential scattering proved that resonant scattering is also a coherent process. In other words, the result obtained evidenced the preservation of phase memory by radiation throughout the entire process of nuclear scattering. The scale of temporal coherence is determined by the duration of the collision of the particle with the nucleus [4]. In the case of resonance on the ^{57}Fe nucleus, which was studied in [5], the time of collision of a gamma quantum with the nucleus at the resonance energy of the quantum was $\sim 10^{-7}$ s. During this time, about 10^{12} phased oscillations of the nuclear transition current occurred. Thus, the process observed in the work cited above is one of the examples of the unique persistence of phase memory.

Somewhat later, in 1963, Bernstein and Campbell [6] observed the total external reflection of Mössbauer radiation from an ^{57}Fe mirror. This experiment was the first evidence that coherent scattering of gamma rays can occur not only on a single nucleus but also on an ensemble of nuclei, i.e., it was a demonstration of spatial coherence of resonant scattering. The existence of spatial coherence was convincingly confirmed by Black and Duerdoth [7] when studying the Bragg reflection of gamma rays by the nuclear lattice of a crystal. The observation of total external reflection and Bragg diffraction — the phenomena in which all scattering centers are involved — proves that many nuclei can be affected by excitation during the scattering of a single photon. In relation to this, a question of fundamental importance arises: in what way can the collective excitation of a nuclear ensemble occur if the photon energy is only sufficient to excite a single nucleus? Should this be the case, the scattering process should be localized at a certain center. It is apparent that the classical approach to describing the diffraction of gamma quanta by nuclei fails to answer this question.

To resolve the contradiction that arose, Trammell [8] and Kagan and Afanas'ev [9] proposed the concept of *delocalized nuclear excitation*. This idea, which is quite natural in its essence, is based on the observation that, during elastic scattering in the nuclear ensemble, no mark is left that would label an individual nucleus participating in the scattering. Given this fact, it can be assumed that, in accordance with the quantum mechanical principle of superposition of states, each nucleus in the scattering system is excited with a certain probability amplitude. In this case, the elementary state is one in which one of the nuclei is excited, while the rest are not. As for the wave function of delocalized excitation, it represents a linear superposition of elementary excitations. In this representation, it is as if the gamma quantum is shared by the nuclei of the entire ensemble, with the spatiotemporal correlation of the phases of nuclear excitations being maintained. The superposition excitation state is the one that we call a nuclear exciton (the term was introduced by Zaretsky and Lomonosov [10]). It is apparent that, in the proposed interpretation under consideration, the scattering process is of a collective nature. In accordance with these properties of nuclear excitation, elastic scattering of a gamma quantum by an ensemble of nuclei in a crystal should be considered a macroscopic quantum mechanical phenomenon. In this process, the crystal operates as a kind of macroscopic quantum resonator.

We have seen that the nuclear exciton is by its nature associated with nuclear transition currents. Hence, it is clear why its existence provides a physical basis for the use of macroscopic polarization of nuclei in describing radiative nuclear phenomena in Maxwell's equations. The polarization of a nuclear ensemble is a sum of the induced electrical and magnetic moments of nuclear transitions in a unit volume. The induced moments are apparently determined by the multipolarity of nuclear transitions. The connection between the nuclear exciton and macroscopic polarization indicates that Maxwell's equations in their classical form can be used for the theoretical analysis of coherent nuclear resonant scattering.

It is clear that nuclear transition currents cannot exist separately from the electromagnetic field of radiation. These two subsystems should form a single physical entity. The radiation field and nuclear currents interact with each other and exchange energy. Both propagate through the target as a coupled state of nuclear polarization and electromagnetic waves. Following the terminology adopted in optics, the coupled system of field and currents inside the target was called the nuclear exciton-polariton, or simply nuclear polariton [11–16]. Nuclear polaritons exist in a crystal in the form of both traveling and standing waves. Temporal and spatial phase relationships of the nuclear polarization and field are realized throughout the crystal. They drive the formation of the wave field within the crystal and at the exit from it. Approaching the crystal boundary, the nuclear polariton generates a coherent beam of radiation in certain directions, and coherent fluorescence of the nuclei is observed.

Collective nuclear scattering dominates in the entire picture of the interaction of gamma radiation with the nuclear ensemble. In generating a nuclear polariton, an ensemble of nuclei operates like a macroscopic resonator, the resonant properties of which differ quantitatively and qualitatively from those of an individual nucleus. The parameters characteristic of an individual resonant interaction, such as linewidth, lifetime, and the ratio of the probabilities of elastic and inelastic scattering, undergo radical changes.

With the discovery of the Mössbauer effect, a new direction in theoretical and experimental optics — quantum optics of resonant gamma radiation, or briefly gamma optics — emerged and began developing. It covers a wide range of coherent phenomena with resonant gamma radiation in both energy and temporal spaces. Since 1960, many research teams worldwide have invested enormous effort in gaining knowledge and developing applications in the new field. It would be difficult in one review to present the formation of a new field of knowledge and assess the

achievements scientists have made in this area. To date, a fair number of reviews have been published. Here, we mention only a few of them [17–22, 26, 27].

One important application of coherent nuclear fluorescence physics is the creation of a source of synchrotron Mössbauer (SM) radiation. The topic of this review is precisely the history of the creation of such a source, a description of its physical basis, and a presentation of the increasingly popular field of Mössbauer spectroscopy, in which such a source is used. We display to readers the most impressive results obtained using SM radiation and its promising applications.

2. Physical basis

2.1 Coherent enhancement of the radiative channel of nuclear resonant scattering

The ideas of the dynamic theory of scattering, formulated by Ewald, are based on the dynamic interaction of radiation with atoms of matter, in which, as a result of multiple scattering, an equivalent exchange of energy is realized between the excited atomic currents and the radiation field. As a result of such an exchange, a well-established dynamic self-consistency between the field and currents arises. The dynamic theory of X-ray scattering by crystals was created in the works of Ewald, Laue, and other researchers [23–25].

Shortly after Mössbauer's discovery, in a series of studies by Kagan and Afanas'ev and Trammell and Hannon, presented in reviews [26, 27], the dynamic theory of nuclear resonant scattering of gamma radiation was developed. Kagan and Afanas'ev predicted two surprising effects: suppression of inelastic channels of a nuclear reaction [28] and total reflection of gamma radiation in nuclear resonant Bragg scattering [29]. These phenomena are surprising because, in radiative transitions in nuclear isomers, in most cases, it is the internal electron conversion channel that dominates. Even in such seemingly insurmountable natural conditions, both of the mentioned theoretical works predicted the feasibility of an extraordinary enhancement of the radiation channel of coherent scattering of gamma radiation in ideal crystals. We now consider this issue in more detail using the example of two-wave diffraction.

In two-wave diffraction, the wave field in a crystal is a coherent superposition of waves scattered in the primary and in the only allowed Bragg directions. The solution of the dynamic problem shows that the wave field in a crystal under certain conditions takes the form of a standing wave, whose amplitude and polarization are modulated in the direction perpendicular to the reflecting planes. To suppress the inelastic channel, it turns out that it is not at all necessary for the field to contain nodal planes with zero strength at the locations of the atoms (Fig. 4 in [30]), as is the case in X-ray diffraction [25]. In the angular dependence of nuclear resonance scattering, when approaching the Bragg angle, the reflectivity of the crystal can tend to unity, i.e., to one hundred percent reflection [29], while *the amplitude of nuclear excitation tends to zero* [28]. Here, we encounter a seemingly paradoxical situation: total reflection occurs at the moment when the excitation of the nuclei disappears. How can this paradox be resolved?

An analysis of the solutions to the dynamic theory reveals that the approach to the Bragg angle is accompanied by an increase in the depth to which radiation penetrates into the crystal. The characteristic penetration depth, and therefore the number of nuclear planes N involved in the absorption and diffraction of radiation, turns out to be inversely proportional to the square root of the deviation of the angle of incidence of radiation from the Bragg angle $\Delta\theta$ [30]:

$$N \sim \frac{1}{\sqrt{|\Delta\theta|}} .$$

In quantitative terms, the absorption and diffraction of radiation by nuclei are determined not only by the number of nuclear planes participating in the interaction but also by the amplitude of excitation of nuclei on these planes. As for the latter, it turns out to be directly proportional to the root of the angular deviation:

$$A \sim \sqrt{|\Delta\theta|} .$$

We see that a decrease in the amplitude of excitation of nuclei is accompanied by an increase in the number of nuclear planes in approaching the Bragg angle. We now compare the scale of absorption of radiation and scattering of radiation by nuclei under these conditions. When absorption is calculated, the contributions of nuclei to it are summed up in an incoherent manner, so for total absorption we obtain

$$\text{Absorption} \sim N(A)^2 \sim \left(\frac{1}{\sqrt{|\Delta\theta|}}\right)|\Delta\theta| = \sqrt{|\Delta\theta|} , \qquad (1)$$

i.e., absorption is proportional to the root of the angle, and exactly at the Bragg angle it completely vanishes. This is precisely the effect of suppressing the conversion channel. When diffraction is considered, the contributions to scattering from all nuclei should be coherently added. Thus, reflection is determined by the square of the total amplitude of scattering by each nuclear plane:

$$\text{Reflection} \sim (NA)^2 \sim \left|\frac{1}{\sqrt{|\Delta\theta|}}\sqrt{|\Delta\theta|}\right|^2 = 1 . \qquad (2)$$

What do we obtain? Despite the disappearance of the excitation of nuclei by the wave field, the reflection not only does not vanish but becomes total when approaching the Bragg angle. Apparently, such an amazing result is due to the coherent enhancement of nuclear resonant scattering. In a semi-infinite crystal, radiation can only exit from where it entered, i.e., through the surface of the crystal. Therefore, when radiation penetrates infinitely deep into the crystal, its total reflection is observed. The size of the angular region in which enhancement of the radiative channel is observed is determined by the scattering amplitude. Since the amplitude of Mössbauer nuclear resonance scattering is very large (it can exceed the amplitude of electron Rayleigh scattering by an order of magnitude), the dominance of the radiation channel over the conversion channel is observed in very large angular intervals, in real cases on the order of 50 μrad.

2.2 Pure nuclear diffraction

As mentioned above, the electromagnetic field of gamma radiation interacts not only with atomic nuclei but also with the electron shell of atoms. The interference of elastic scattering on two subsystems in a crystal has been studied as a physical phenomenon by several research teams [6, 31–33]. Due to electron-nuclear interference, the shape of the nuclear

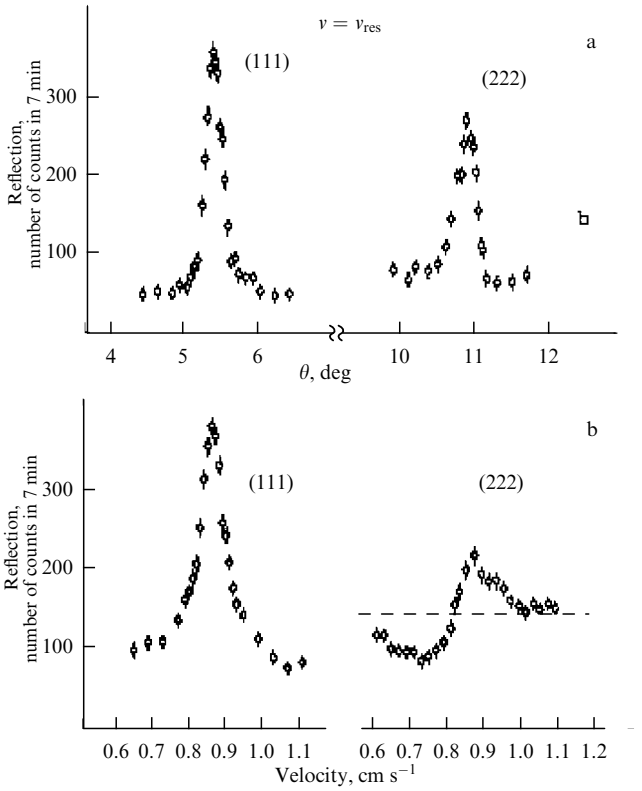

Figure 1. (a) Angular and (b) energy dependences of the reflection of 14.41-keV gamma radiation from a hematite crystal upon excitation of the nuclear transition $-1/2 \rightarrow -3/2$ (from [34]).

resonance turns out to be strongly dependent on the relation of the amplitudes and phases of nuclear and electron scattering. In the electron scattering channel, these two parameters can be considered invariable in the region of nuclear resonance, but in the nuclear channel both characteristics alter radically when passing through resonance. The phase changes by an amount of π, and the amplitude sharply passes through its maximum value at resonance. Due to phase relationships, the amplitudes of nuclear and electron scattering constructively add on one side of the resonance and destructively on the other. As a result, the resonance dependence of the scattering intensity takes on a dispersive form, the shape of a Fano resonance. The sign of dispersion and dispersion contrast are determined by many factors, including the crystal structure and the structure of intracrystalline fields.

However, it is quite clear that the presence of electron scattering can significantly complicate the study of the properties and characteristics of coherent nuclear resonance fluorescence. In particular, in the scattering of synchrotron radiation, which is broadband compared to the width of the nuclear resonance, the signal from the nuclei is obscured by the overwhelming background of nonresonant radiation. In overcoming these difficulties, the discovery of purely nuclear diffraction played a decisive role.

Figure 1 shows the results of the first observation of purely nuclear diffraction of resonant gamma radiation [34]. This phenomenon was discovered in studying Bragg reflections of 14.4 keV gamma rays from antiferromagnetic hematite crystal $^{57}Fe_2O_3$ grown on the basis of a resonant isotope of iron. Figure 1a shows the angular dependences of the intensity of reflected radiation in the vicinity of the Bragg angles for reflections (1 1 1) and (2 2 2) in hematite. The energy of the incident radiation corresponded to the excitation of the nuclear transition $-1/2 \rightarrow -3/2$ in the Mössbauer spectrum of the crystal. Figure 1b shows the energy dependences of the intensity of reflected radiation in the region of the above-mentioned resonance at fixed angles for reflections (1 1 1) and (2 2 2). The shapes of the resulting resonance curves were strikingly different. In reflection (1 1 1), a symmetrical maximum was observed, while in reflection (2 2 2), a pronounced dispersion curve was revealed. This observation was evidence of the purely nuclear nature of reflection (1 1 1) in comparison to the interference, electron-nuclear nature of reflection (2 2 2). The possibility of obtaining magnetic maxima in the diffraction of gamma rays, by analogy with magnetic maxima in neutron scattering, was pointed out by Trammell [8]. The possibility of obtaining purely nuclear diffraction in presence of magnetic and quadrupole splitting of nuclear levels was theoretically justified by Belyakov and Aivazyan [35, 36]. The first searches for nuclear maxima of both types were carried out in [34, 37, 38]. In later studies, to obtain purely nuclear diffraction, including the scattering of synchrotron radiation, antiferromagnetic iron borate crystals, which feature a number of advantages over hematite, were used [39].

We now illustrate the nature of the occurrence of purely nuclear diffraction in an antiferromagnetic crystal using a simple setup. In an antiferromagnetic iron borate crystal, $FeBO_3$, the magnetic field strength vectors $\mathbf{H}_1$ and $\mathbf{H}_2$ on the iron nuclei included in the unit cell of the crystal have opposite directions (Fig. 2). When radiation is scattered by atoms of the ^{57}Fe isotope under nuclear resonance conditions, excitation of currents of the M1 multipole in nuclei and E1 multipole in electron shells is observed. Since the local magnetic fields on two cell nuclei are oriented in opposite directions, at the same resonant energy of incident radiation in the nuclei, transitions are excited, characterized by opposite magnetic quantum numbers $M = \pm 1$, and circular right- and left-polarized currents are accordingly excited. However, identical linearly polarized currents are excited in the electronic shells (Fig. 2a and 2b, respectively). If structurally forbidden Bragg reflections are used, which in our case is the (111) reflection, a phase difference of π radians arises between the waves scattered on two atoms of the cell. As a result, partial waves scattered by the electron shells of atoms add up destructively, i.e., cancel each other out (Fig. 2b). However, the circularly polarized waves scattered by the nuclei add up in such a way that a linearly polarized wave of double amplitude is formed (Fig. 2a). In this case, the polarization of the scattered wave turns out to be orthogonal to that of the incident wave. In our example, the π-polarized wave is transformed into a σ-polarized wave. It should be noted, that the transformation of the polarization state is effectively employed in experiments using polarization analysis of scattered radiation [55, 56]. If synchrotron radiation is used to excite nuclei, under conditions of purely nuclear diffraction, the scattered radiation only contains the resonant component of the incident radiation. Thus, purely nuclear diffraction makes it possible to generate coherent fully resonant gamma radiation with an energy of 14.41 keV.

Synchrotron radiation is a sequence of short pulses with a duration of ~ 0.5 ns, separated by large time intervals. After excitation of the isomeric state of the ^{57}Fe nucleus by a separate SR pulse, the nuclei begin to glow in and of themselves, which is nuclear fluorescence with a duration on

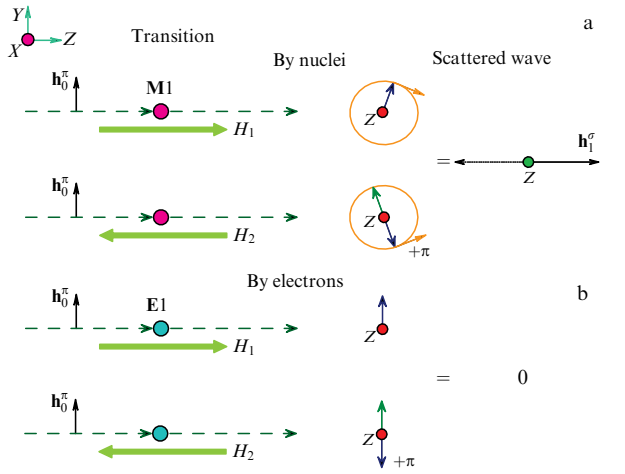

Figure 2. Diagram of scattering of π-polarized gamma radiation on two ^{57}Fe atoms included in unit cell of an antiferromagnetic crystal. Radiation energy is tuned to resonances $\pm 1/2 \rightarrow \pm 3/2$ in Mössbauer spectra of first and second nuclei, respectively. In nuclei (a), circularly polarized magnetic dipole moments of transitions are excited, while in electronic shells of atoms (b), linearly polarized electric dipole moments are excited. In a structurally forbidden reflection, the phase shift of oscillations of excited moments is equal to π radians.

the order of the lifetime of this state. When the conditions of purely nuclear diffraction are fulfilled, fluorescent gamma radiation propagates in a certain direction in a narrow solid angle. While the excitation of nuclei is fueled by synchrotron pulses, the crystal glows and emits resonant gamma rays in these directions throughout the entire irradiation time, i.e., a stationary flow of resonant gamma radiation is formed.

If hyperfine splitting of nuclear levels is large, which occurs at room temperature in an iron borate crystal, the spectrum of fluorescent resonance radiation contains four lines widely spaced from each other. It is apparent that gamma radiation with such a spectrum is very inconvenient, in fact unsuitable, for spectroscopic research. Fortunately, the unique magnetic properties of iron borate make it possible to resolve this problem.

When the crystal is heated to the temperature of the magnetic phase transition, Néel point $T_N = 75.3$ °C, the energies of interaction of the magnetic and quadrupole electric moments in the excited state of the nucleus with the local magnetic and electric fields become comparable. Hyperfine interaction in an excited state acquires a combined character [40, 41, 45]. Due to these circumstances, which are discussed in more detail in Section 2.4, conditions are created when a single line is formed in the spectrum of fluorescent gamma radiation. The energy width of this line is close to the natural width of the nuclear level and amounts to $\sim 5 \times 10^{-9}$ eV. In this case, a unique monochromaticity of gamma radiation is achieved: $\Delta E/E \sim 3 \times 10^{-13}$. In the described process, the crystal acts as a macroscopic quantum mechanical resonator, generating its own radiation with a narrow spectral line — synchrotron Mössbauer radiation — under the influence of broadband synchrotron radiation.

2.3 Multidimensional and multipath gamma radiation interference

Purely nuclear diffraction of gamma radiation in an iron borate crystal has a very complex interference nature. In addition to the well-known interference of X-ray radiation in geometric three-dimensional space, interference in energy and spin spaces is in effect.

In the case of hyperfine splitting of nuclear levels, all allowed nuclear transitions between the ground and excited states are involved in the scattering of any spectral component of radiation. In this case, interference of scattering paths at different resonant transitions, in other words, interference in energy space [42], occurs. The contribution of an individual nuclear transition depends on the difference between the radiation frequency and the resonant frequency of this transition. Apparently, the smaller the distance between the resonant frequencies of transitions, the stronger the manifestation of interference in energy space.

Quite different is interference in spin space, which is quantum mechanical in nature. The solution to the quantum mechanical problem for the excited state of the ^{57}Fe nucleus under conditions of combined hyperfine interaction in an iron borate crystal shows that the nucleus is in states mixed in spin projection [43]. The spin of the nucleus in the excited state is equal to $I = 3/2$; its projection onto the quantum axis, associated with the direction of the magnetic field on the nucleus, takes on the values $m = -3/2, -1/2, +1/2, +3/2$. In an excited state, due to hyperfine interaction, the energy level is split into four sub-levels $e = 1, 2, 3, 4$, which are numbered in order of increasing energy of the sublevels. Due to the interaction of the magnetic and electric quadrupole moments of the nucleus in the excited state with the magnetic and electric fields in the crystal, the wave function describing the state of the nucleus at an individual sublevel of the excited state is the sum of two functions, each of which corresponds to a specific spin projection, as shown in Table 1. In the table, the coefficients $c_e^{m_e}$ represent the amplitudes of the probability of detecting an excited nucleus in a state with the corresponding projection of the nuclear spin at each sublevel.

The elastic scattering of a gamma quantum can be represented as consisting of three stages: excitation of the nucleus with the capture of a gamma quantum, dwelling of the nucleus in an excited state, and de-excitation of the nucleus with the emission of a quantum. Several possibilities are available in a mixed state. A quantum can excite a nucleus into a certain state according to the spin projection and be emitted from the same state, or a quantum can excite a nucleus into one state according to the spin projection and be emitted from another. In total, under conditions of hyperfine interaction in an iron borate crystal, four paths of elastic quantum scattering in spin space are open. An example of scattering along different paths in spin space is shown in Fig. 3 for an individual ^{57}Fe nucleus located in a magnetic field directed along the quantum axis and one of the nuclear transitions.

As can be seen from Fig. 3, along all scattering paths, nuclear transition currents are excited, which are characterized by magnetic quantum numbers $M = \pm 1$, i.e., currents of circular left or right polarization. In the general case, they

Table 1. Natural wave functions of nuclear excited states for four energy sublevels of the ^{57}Fe nucleus in an iron borate crystal.

1	2	3	4
$c_1^{-3/2}\left\vert -\frac{3}{2}\right\rangle + c_1^{+1/2}\left\vert +\frac{1}{2}\right\rangle$	$c_2^{-1/2}\left\vert -\frac{1}{2}\right\rangle + c_2^{+3/2}\left\vert +\frac{3}{2}\right\rangle$	$c_3^{+1/2}\left\vert +\frac{1}{2}\right\rangle + c_3^{-3/2}\left\vert -\frac{3}{2}\right\rangle$	$c_4^{+3/2}\left\vert +\frac{3}{2}\right\rangle + c_4^{-1/2}\left\vert -\frac{1}{2}\right\rangle$

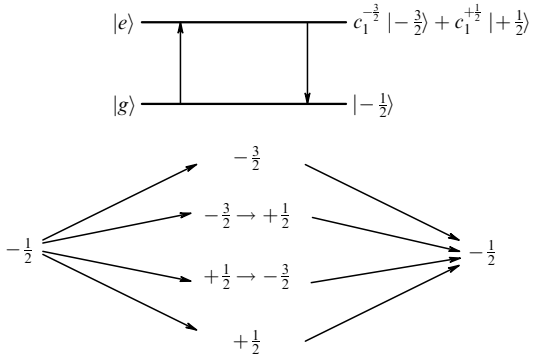

Figure 3. Paths of scattering in spin space upon excitation of one of the transitions of the ^{57}Fe nucleus to the 14.41-keV level. Upper part displays levels between which the transition occurs and corresponding wave functions of spin states.

produce elliptically polarized scattered waves. Interference in spin space is very sophisticated. A separate article is devoted to this phenomenon, where, using the example of gamma radiation scattering on a single nucleus under conditions of combined hyperfine interaction, a strong dependence of the interference conditions on the polarization of the incident radiation and the direction of the crystalline magnetic field on the nucleus — oriented along the quantum axis or in the opposite direction — is found [44].

The multidimensional and multipath pattern of nuclear scattering should be taken into account when calculating the polarizability of a nuclear ensemble. The polarizability of matter is the main parameter in scattering theory. Nuclear polarizability is directly related to the amplitude of nuclear resonant scattering. In an iron borate crystal, the nuclear polarizability can be represented in the following form [45]:

$$\eta_{dd'}^{ss'} = -\frac{3}{KV_0}\,\sigma_0 \rho f_{\mathrm{LM}} \sum_a \exp\left\{\mathrm{i}(\mathbf{k}_{d'} - \mathbf{k}_d)\mathbf{r}_a\right\} \times \sum_{n=1}^{4} \frac{1}{v_n - i} \sum_{m'_e, m''_e} G_n^a(m'_e, m''_e)\,, \tag{3}$$

with parameter $G_n^a(m'_e, m''_e)$ equal to

$$G_n^a(m'_e, m''_e) = \left\langle \frac{1}{2}, m_g; 1, M \middle| \frac{3}{2}, m'_e \right\rangle \left\langle \frac{1}{2}, m_g; 1, M' \middle| \frac{3}{2}, m''_e \right\rangle \times c_e^{m'_e} c_e^{m''_e} (\mathbf{h}_d^s \mathbf{n}_{-M}^a)\,(\mathbf{h}_{d'}^{s'} \mathbf{n}_{-M'}^a)^*\,. \tag{4}$$

The physical parameters in Eqns (3) and (4) are denoted as follows: $K = 2\pi/\lambda$ is the wave number; V_0 is the volume of the unit cell of the crystal; σ_0 is the maximum resonant cross section; ρ is the enrichment of the crystal with the resonant isotope ^{57}Fe; f_{LM} is the recoil-free scattering factor, which is the product of the square roots of the Lamb–Mössbauer factors in the directions d, d'; $\mathbf{k}_d$ and $\mathbf{k}_{d'}$ are the wave vectors of the incident and scattered waves; s, s' are the polarizations of these waves, respectively; $\mathbf{r}_a$ is the coordinate of the atom in the unit cell of the crystal; $v_n = (E - E_n)/(\Gamma_0/2)$ is the deviation in the energy of the incident radiation from the resonance in units of the natural half-width of the resonance; $\langle 1/2, m_g; 1, M | 3/2, m_e\rangle$ are the Clebsch–Gordan coefficients, the product of which characterizes the probability of transition between sublevels of the ground and excited states (taking into account the transfer of angular momentum in the system nucleus + gamma quantum); m_g and m_e are the projections of the nuclear spins on the sublevels of the ground and excited states; $c_e^{m'_e} c_e^{m''_e}$ are the amplitudes of the spin states on the sublevels of the excited state; the parentheses $(\mathbf{h}^s \mathbf{n}_{-M})$ and $(\mathbf{h}^{s'} \mathbf{n}_{-M'})^*$ represent scalar products of the vectors of magnetic polarization of radiation and unit vectors characterizing the spatial properties of the magnetic moment of the nuclear transition at the stages of nucleus excitation and de-excitation; and for the quantum axis oriented along the Z axis, we have $\mathbf{n}_{\pm 1} = \mp 1/\sqrt{2}\,(\mathbf{n}_x \pm \mathrm{i}\mathbf{n}_y)$.

Equation (3) is a triple sum representing the coherent addition of scattering paths in the three spaces mentioned above. For each nucleus in the unit cell and a separate transition in this nucleus between the ground and excited states, the amplitudes are summed along the scattering paths in spin space shown in Fig. 3. This procedure is repeated for all other energy transitions allowed in a given nucleus. Then, the same operations are performed for another nucleus of the unit cell. In total, the cell of the crystal under consideration contains two iron nuclei, in each of which the selection rules for the magnetic dipole transition M1 allow four nuclear transitions, characterized by magnetic quantum numbers $M = \pm 1$. For each transition, four scattering paths are available in spin space. Thus, in the scattering process under consideration, we are dealing with the interference of 32 scattering paths in three spaces.

In the case of purely nuclear diffraction of radiation in an iron borate crystal, the nuclear polarizability $\eta_{dd'}^{ss'}$ is represented by a (2×2) matrix,

$$\eta_{dd'}^{ss'} = \begin{vmatrix} \eta_{00}^{ss} & \eta_{01}^{ss'} \\ \eta_{10}^{s's} & \eta_{11}^{s's'} \end{vmatrix}, \tag{5}$$

where each of the indices s, s' denotes the π- or σ-polarization of the radiation. Table 2 shows the nuclear polarizability

Table 2. Matrices of nuclear polarizability of iron borate for reflection (3 3 3).

Nuclear resonance	1	3	4	6
330 kOe $\beta = -1$, incident π-polarized radiation				
Position of resonance (Γ)	−53.78	−9.45	7.50	55.73
$\begin{Bmatrix} \eta_{00}^{\pi\pi} & \eta_{01}^{\pi\sigma} \\ \eta_{10}^{\sigma\pi} & \eta_{11}^{\sigma\sigma} \end{Bmatrix}$	$\begin{Bmatrix} -22.41 & 22.58\mathrm{i} \\ -22.58\mathrm{i} & -22.74 \end{Bmatrix}$	$\begin{Bmatrix} -6.81 & -7.50\mathrm{i} \\ 7.50\mathrm{i} & -8.25 \end{Bmatrix}$	$\begin{Bmatrix} -6.89 & 7.50\mathrm{i} \\ -7.50\mathrm{i} & -8.17 \end{Bmatrix}$	$\begin{Bmatrix} -22.50 & -22.59\mathrm{i} \\ 22.59\mathrm{i} & -22.67 \end{Bmatrix}$
2 kOe $\beta = -1$, incident π-polarized radiation				
Position of resonance (Γ)	−2.08	**1.7**	−1.84	**2.22**
$\begin{Bmatrix} \eta_{00}^{\pi\pi} & \eta_{01}^{\pi\sigma} \\ \eta_{10}^{\sigma\pi} & \eta_{11}^{\sigma\sigma} \end{Bmatrix}$	$\begin{Bmatrix} -0.03 & 0.85\mathrm{i} \\ -0.85\mathrm{i} & -22.59 \end{Bmatrix}$	$\begin{Bmatrix} -6.97 & 14.23\mathrm{i} \\ -14.23\mathrm{i} & -29.04 \end{Bmatrix}$	$\begin{Bmatrix} -0.03 & 0.77\mathrm{i} \\ -0.77\mathrm{i} & -21.04 \end{Bmatrix}$	$\begin{Bmatrix} -8.65 & -15.85\mathrm{i} \\ 15.85\mathrm{i} & -29.04 \end{Bmatrix}$

matrices of an iron borate crystal in the geometry of symmetrical Bragg reflection for two values of the magnetic field on the nuclei of 330 kOe and 2 kOe and incoming π-polarized radiation. A hyperfine magnetic field of 2 kOe is realized near the magnetic phase transition from the antiferromagnetic to the paramagnetic state, the Néel point. Noteworthy is the significant anisotropy of nuclear polarizability in a field of 2 kOe, which is absent in a field of 330 kOe.

The matrices are calculated for four nuclear resonances, which are not prohibited in purely nuclear diffraction in an iron borate crystal. The resonances correspond to lines 1, 3, 4, and 6 in the Mössbauer spectrum of the ^{57}Fe nucleus in the magnetic splitting of nuclear levels. Since the local magnetic fields on the nuclei in the unit cell of the crystal are antiparallel, these resonances correspond to transitions between states of the nuclei in which signs of the spin projections are opposite.

2.4 On the peculiarities of nuclear resonant diffraction

The dynamic theory of nuclear resonant scattering of gamma rays was developed in a series of studies by Kagan, Afanas'ev, and Perstnev, which started in 1965 [28, 29, 46]. It was in essence a semiclassical theory, in which quantum mechanical methods were used to calculate the nuclear amplitude, while the problem of dynamic scattering of gamma radiation in a crystal was solved using Maxwell's equations. Beginning in 1968, Trammell and Hannon published a series of papers on dynamic nuclear resonance scattering of gamma radiation, in which methods of quantum electrodynamics were applied [47–49]. Currently, both theories are very popular and widely used.

We now consider the distinctive features of nuclear resonance diffraction. In coherent optics of X-rays, all the main events of interference and diffraction of radiation occur in geometric three-dimensional space. The main calculated and measured characteristics are the angular dependences of the intensity of diffraction reflection of radiation by crystals. This situation is due to the fact that the amplitude of X-ray scattering by atoms far from the absorption edges does not depend on the frequency of the incident radiation. On the contrary, in the case of nuclear scattering, the amplitude and polarizability are resonant in nature and strongly depend on the radiation frequency (see Eqn (3)). In the diffraction of gamma radiation in the Bragg geometry, the reflectivity of the crystal is determined by the following formula derived using theory [29]:

$$Q = |R|^2 \frac{1}{|\beta|}\,, \tag{6}$$

where R is the reflection coefficient and β is the reflection asymmetry factor; $\beta = -\sin\theta_0/\sin\theta_1$, where θ_0 is the grazing angle of the beam incident on the crystal, and θ_1 is the grazing angle of the reflected beam. For a crystal semi-infinite in thickness, the reflection coefficient has the form

$$R = -\frac{\beta\tilde{\eta}_{10}}{2\varepsilon_0^{(1)} - \tilde{\eta}_{00}}\,. \tag{7}$$

The formula above contains the following physical quantities and parameters: elements of the polarizability matrix of the scattering system $\tilde{\eta}_{00}$ and $\tilde{\eta}_{10}$, in which electronic polarizability is added to the nuclear polarizability; β is the asymmetry factor defined above; and $\varepsilon_0^{(1)}$ is a small complex addition to the refractive index, determined by the following formula:

$$\varepsilon_0^{(1)} = \frac{1}{4}\left\{\tilde{\eta}_{00} + \beta\tilde{\eta}_{11} - \alpha\beta - \sqrt{(\tilde{\eta}_{00} - \beta\tilde{\eta}_{11} + \alpha\beta)^2 + 4\beta\tilde{\eta}_{01}\tilde{\eta}_{10}}\right\}, \tag{8}$$

which, in addition to the elements of the polarizability matrix of the crystal, includes the angular parameter α directly related to the deviation from the Bragg angle: $\alpha = -2\sin 2\theta_B(\theta - \theta_B)$, where θ_B is the Bragg angle. Nuclear polarizability, as shown above (Eqn (3)), depends on the energy of the incident radiation relative to the resonant one. It follows from the said that the strength of diffraction reflection of gamma rays from the nuclear lattice of a crystal depends not only on the angle of incidence of the rays in the vicinity of the Bragg angle but also on the energy of the radiation exciting the nucleus. Consequently, the reflectivity of the crystal looks like a surface of complex shape, located above the zero-level plane in angle–energy coordinates. Currently, reflections (1 1 1) and (3 3 3) in an iron borate crystal are used to obtain SM radiation. The (1 1 1) planes extend onto the surface of the plate crystal, so these reflections are classified as symmetric, for which the angle of incidence is equal to the angle of reflection. Figure 4 shows the landscape of the crystal reflectivity for the (3 3 3) reflection in the nuclear resonance region at a temperature near the Néel point and in the vicinity of the Bragg angle. The reflectivity landscape is formed by multispatial and multipath interference of gamma radiation in geometric, energy, and spin spaces [44, 45]. The reflectivity surface Q has a rather complicated shape. The cross section of the surface at a given angle of incidence of rays on the crystal represents the energy dependence of reflection in the resonant region at the selected angle of incidence. For example, at an incidence angle of 100 μrad, the cross section has the shape of a single resonance (orange section in Fig. 4).

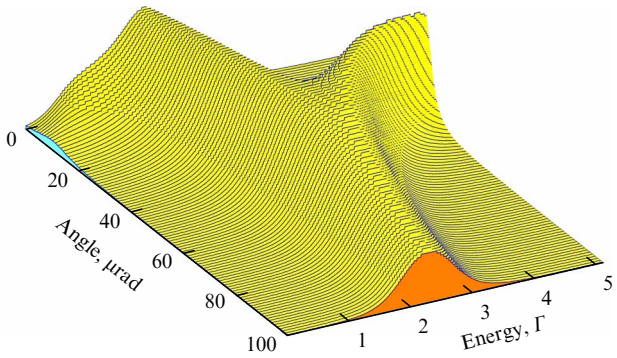

Figure 4. Landscape of reflectivity Q of crystal $^{57}FeBO_3$ for symmetric reflection (333) in the vicinity of the Bragg angle and in the nuclear resonance region with a field on nuclei of 2 kOe. Energy scale spans the region of 5 Γ, where Γ is the natural width of the nuclear level in the first excited state of the ^{57}Fe nucleus. Angular scale covers an interval of 100 rad in the vicinity of the Bragg angle.

2.5 Interplay between the Anisotropy of Polarizability of Nuclei and the Asymmetry of Diffraction Geometry

We begin by considering the case of no anisotropy of nuclear polarizability in an iron borate crystal. This condition is satisfied at room temperature. The magnetic field on iron nuclei at a given temperature is approximately 330 kOe. Due to the hyperfine splitting of nuclear levels in such a strong field, the nuclear resonances in the Mössbauer spectrum of

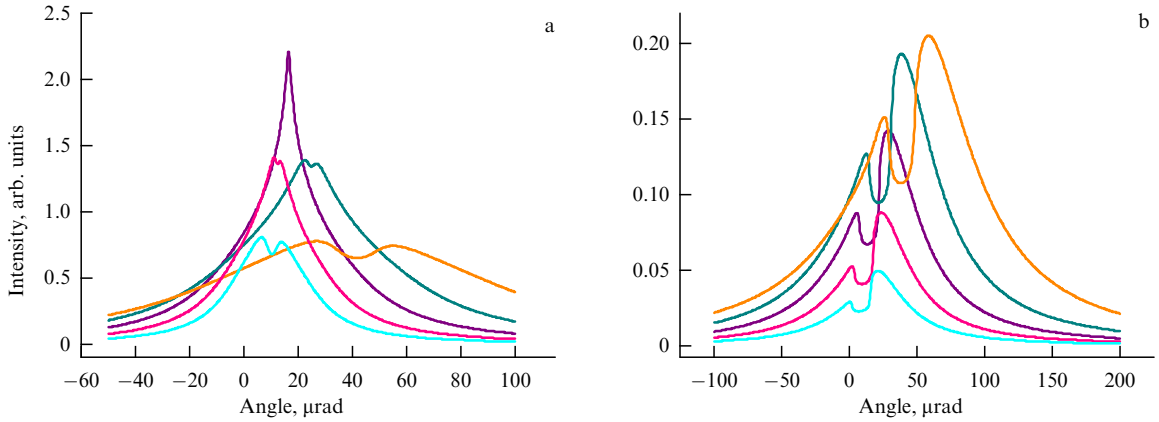

Figure 5. Angular dependences of the intensity of purely nuclear diffraction of π-polarized synchrotron radiation from a $^{57}FeBO_3$ crystal in reflection (333) for local magnetic fields on nuclei of (a) 330 kOe and (b) 2 kOe and for various asymmetry factors. Horizontal axis represents angle of deviation from the Bragg position of the crystal. In a field of 330 kOe, the integral over energy is taken in the vicinity of the 6th resonance; in a field of 2 kOe, in the resonance region from $-7\,\Gamma$ to $+10\,\Gamma$. Symmetric case of diffraction, $\beta = -1$, corresponds to purple curves, asymmetric cases, $\beta = -0.5$, dark blue; $\beta = -0.25$, orange; $\beta = -2.0$, pink; and $\beta = -4.0$, blue, respectively.

iron borate are highly separated, practically isolated from each other. The minimum distance between them is $17\,\Gamma$. In this case, the following relations between the matrix elements of nuclear polarizability hold for all resonances: $\eta_{00}^{\pi\pi} \approx \eta_{11}^{\sigma\sigma}$ and $\eta_{00}^{\sigma\sigma} \approx \eta_{11}^{\pi\pi}$ (see Table 2) (similar relations persist for field 330 kOe, also in an asymmetric diffraction geometry). Consider the reflection (3 3 3) from an iron borate crystal. Figure 5a shows the angular dependences of the reflection intensity of π-polarized synchrotron radiation upon excitation of the 6th nuclear resonance. Integration over energy was carried out in the vicinity of the 6th resonance in the interval of $55.73\,\Gamma \pm 1.5\,\Gamma$. The dependences for various asymmetries of diffraction scattering in the Bragg geometry are compared. The figure shows angular distributions in both symmetric and asymmetric geometries. The latter correspond to the asymmetry factors $|\beta| < 1$ for shallow ray incidence and the asymmetry factors $|\beta| > 1$ for steep ray incidence. As can be seen from Fig. 5a, in the case of shallow ray incidence, with increasing asymmetry, the angular dependence broadens significantly and shifts towards larger angles. On the contrary, with increasing asymmetry at a steep incidence, the dependence narrows and shifts towards smaller angles. It should be noted that the reflection intensity decreases with deviation from the symmetrical geometry both in the direction of shallow and steep incidence.

We now proceed to the case of strong anisotropy of nuclear polarizability. As has already been mentioned, such anisotropy occurs under conditions of hyperfine interactions of the nucleus with magnetic and electric fields in iron borate that are comparable in energy. These conditions are realized in the vicinity of the Néel point. We make here a small digression to present an amazing feature of purely nuclear diffraction in the crystal under consideration discovered in [40, 41].

If iron borate is heated to the Néel temperature, nuclear diffraction vanishes due to the transition of the crystal to a paramagnetic state and, consequently, the destruction of antiferromagnetism in the crystal, which, as we saw above, underlies the existence of purely nuclear diffraction. If, however, a small magnetic field, on the order of 10–100 Oe, is applied to the crystal, nuclear reflection is restored in the form of a single maximum in the energy spectrum (Fig. 2 in [41]). The magnetic fields on the nuclei and their antiferromagnetic ordering are apparently restored. The shape of the spectrum under such conditions corresponds to a combined hyperfine interaction. In a magnetic field of approximately 2 kOe, the interaction energies of the magnetic and electric quadrupole moments of the nucleus with intracrystalline fields become comparable. If a nuclear system is excited by synchrotron radiation, the shape of the spectrum of the generated gamma radiation is described under these conditions by the quadratic Lorentz function [45]. It is the considered remarkable feature of the crystal that makes it possible to obtain SM radiation containing a single line in its spectrum. The reflection function landscape corresponding to these conditions is shown above (see Fig. 4). As can be seen from the figure, to obtain a single-line gamma-ray spectrum, the synchrotron radiation beam should be directed and maintained in the region of the right slope of the angular distribution of the reflection function.

Under the described conditions of hyperfine interaction between the matrix elements of the nuclear polarizability of iron borate, the following relation is valid for the incoming π-polarized radiation: $\eta_{00}^{\pi\pi} \ll \eta_{11}^{\sigma\sigma}$ (see Table 2). Figure 5b compares the angular dependences under these diffraction conditions for the same diffraction scattering geometries as in Fig. 5a. The energy integral is taken in the vicinity of nuclear resonance at the considered temperature from $-7\,\Gamma$ to $+10\,\Gamma$.

Noteworthy is the fact that, in the case of anisotropy of nuclear polarizability, a strong asymmetry of the reflection intensity is observed during the transition from the shallow geometry of Bragg scattering to the steep one. Namely, the reflectivity sharply decreases in the direction of steep incidence of rays, where the asymmetry factor is $|\beta| > 1$, and increases significantly with a shift towards shallow incidence, where $|\beta| < 1$. Undoubtedly, this property of purely nuclear diffraction in an iron borate crystal should be taken into account in the search for the generation of the most intense synchrotron Mössbauer radiation.

Figure 6 shows the spectra of coherent gamma radiation generated in an iron borate crystal when it is irradiated with a continuous series of synchrotron pulses. In one case, a symmetric reflection (3 3 3) is used, and in the other, asymmetric reflection (3 3 11) (see details in [50]). The advantage of asymmetric reflection in the conditions under consideration is

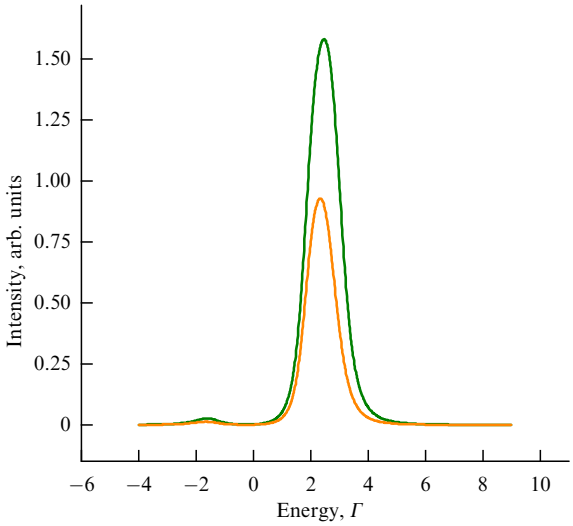

Figure 6. Spectra of gamma radiation emitted by an $^{57}FeBO_3$ crystal upon excitation of iron nuclei by synchrotron π-polarized radiation. Radiation is incident on the crystal in the vicinity of the Bragg asymmetric reflection (3 3 11) in the shallow incidence geometry (green peak). Incidence angle is fixed on right slope of angular curve (Fig. 5b). Local magnetic field on nuclei is 2 kOe. Spectrum for reflection (3 3 3) in symmetric diffraction geometry $\beta = -1.0$ is displayed as an orange peak.

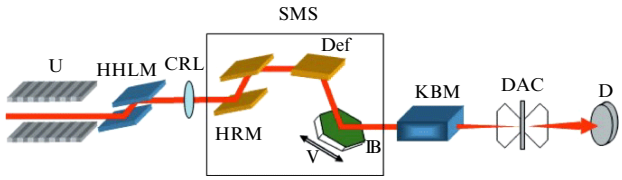

Figure 7. Optical line with a source of synchrotron Mössbauer radiation: U — undulator; HHLM — front-end cooled monochromator; CRL — compound refractive lenses; SMS — SM radiation source that includes an HRM, a high-resolution monochromator, Def — a radiation deflector, and V — a Mössbauer vibrator driving the chamber of the iron borate crystal; KBM — Kirkpatrick–Baez focusing mirrors; DAC — diamond high-pressure chamber (or another sample device); D — photodiode radiation detector (diagram taken from [54]).

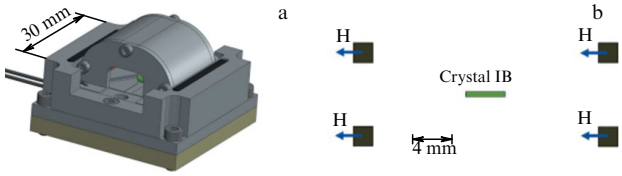

Figure 8. (a) General view of the chamber of the SM radiation source; (b) location of four permanent magnets relative to the iron borate crystal plate (diagram taken from [54]).

clearly visible. By using this reflection, the intensity of coherent gamma radiation could be significantly enhanced.

3. Sources of synchrotron Mössbauer radiation

The first source of synchrotron Mössbauer radiation of ^{57}Fe was created in 1997 [51, 52]. Currently, two sources of SM radiation in the world operate on a continuous basis: one at the Japanese Photon Factory, SPring8 [53], and the other, at the European Synchrotron Radiation Facility (ESRF) [54]. A third source is under testing at the Hamburg-based German accelerator center DESY (private communication). Figure 7 shows a diagram of an optical line with an SM radiation source operating at the ESRF. As an example, a setup is displayed where an SM source is used to study samples under high pressure. We skip the design of optical line elements except for the SM source and only briefly list their purpose and functionality. When a bunch of accelerated electrons flies through the undulator used in the line, X-ray radiation is generated, the spectrum of which contains the components that can excite the nuclei of the ^{57}Fe isotope. However, the undulator radiation spectrum is too broad to direct such radiation directly to the crystal to excite nuclei. The thermal load on the iron borate crystal would be so high that it simply will be destroyed. Therefore, a whole system of monochromators is required to restrict the undulator radiation spectrum while preserving the resonant component in it. All monochromators are made of silicon crystals, the operation of which is based on the principle of Bragg diffraction. The first stage of monochromatization involves crystals with a special cooling system that protects them from overheating and, as a result, possible destruction. Deployed downstream is a set of refractive lenses that reduce the angular divergence of the beam entering the block of SM-source. In this block, the beam is first repeatedly reflected in a system of high-resolution silicon monochromators, which radically narrow the radiation spectrum (to approximately 15 meV). At the last stage, a reflector crystal is used to ensure the beam of radiation emitted by the nuclei is directed along the horizontal optical axis. Kirkpatrick–Baez focusing mirrors are installed on this axis. SM radiation that has interacted with the sample under study is recorded by a photodiode detector.

We now consider in more detail the chamber of iron borate crystal, where coherent gamma radiation is directly generated. As mentioned above, to create conditions for generating radiation with a single-line spectrum, the crystal should be heated to the Néel temperature, $T_N = 75.3\,^{\circ}C$. In addition, an external magnetic field should be used to restore in the crystal local fields with the antiferromagnetic ordering necessary for purely nuclear diffraction. To prevent inhomogeneous broadening of the spectral line of radiation emitted by nuclei, very stringent requirements should be fulfilled regarding the spatial uniformity of the temperature over the crystal and the magnetic field applied to it. Figure 8a shows a general view of the crystal chamber in which the necessary conditions were realized. The chamber design is optimized to obtain a uniform temperature distribution. The internal volume is heated by a thermal foil distributed over the entire internal surface of the chamber. The foil is heated by an electric current passing through it. To suppress air convection, the chamber volume is completely insulated. The windows for radiation entry and exit are covered with Kapton foil. The temperature gradient inside the chamber does not exceed 0.15 K mm^{-1}. The temperature inside the chamber is controlled using a platinum PT100 thermocouple. Temperature instability is maintained within 0.01 K.

The magnetic field applied to the crystal should be highly uniform, since its variations are accompanied by changes in the local field on the nucleus and the associated hyperfine interaction energy [40]. A change in the latter is reflected, in turn, in the spectrum of the generated gamma radiation, in particular, the shape and width of its resonance line.

The field on the crystal is created by a set of four symmetrically located Nb_2Fe_{14} magnets (Fig. 8b). The crystal is installed at the center of symmetry of the magnetic system.

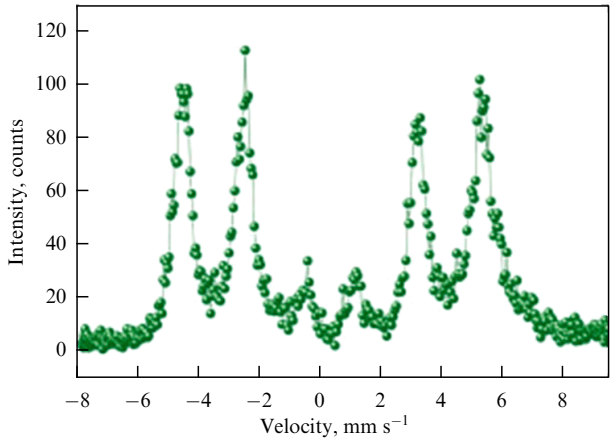

Figure 9. Mössbauer spectrum of an ^{57}Fe layer 8 nm thick, measured in the geometry of grazing incidence of SM radiation for 5 min (from [54]).

The average field on the nucleus is 110 Oe with variations over the crystal of less than 4 Oe. Under these conditions, when a beam of synchrotron radiation incident on the crystal is fixed in the region of the right slope of the angular dependence of reflection, gamma radiation is generated, the spectrum of which consists of a single line $\sim 2\,\Gamma$ wide.

Doppler modulation of the energy of the radiation generated by the crystal is carried out using a Mössbauer vibrator, which drives the entire crystal chamber. Translational motion occurs along an axis lying in the scattering plane and coinciding with the surface of the crystal. This modulation method was proposed in the work of Japanese physicists [53]. With this technique, the beam emitted by the crystal does not shift in space and can be localized on a certain part of the sample under study.

The SM radiation source has a number of important advantages over a laboratory source. The first feature is that the SM radiation spectrum does not contain a recoilless component. Due to the absence of a nonresonant background, the depth of the resonance lines in the absorption spectra, which is referred to as the resonance effect, increases significantly. This circumstance makes it possible to study samples containing a negligible amount of a resonant isotope. No less important is the fact that it becomes possible to significantly (by a factor of $\sim 10^3$) reduce the measurement time with conventional samples while obtaining the same accuracy of spectrum parameters. The exceptional capabilities of the SM source can be illustrated using the Mössbauer spectrum of SM radiation scattering by an 8-nm-thick ^{57}Fe layer deposited on a flat MgO substrate (Fig. 9). The grazing angle of the beam incident on the film was 0.35°, slightly greater than the critical angle of total external reflection. As can be seen, the intensity in nuclear resonances significantly exceeded the base level. Therefore, obtaining the spectrum with good statistical accuracy was a matter of no more than five minutes.

Since the synchrotron radiation exciting the nuclei is almost completely linearly polarized, the radiation emitted by the nuclei is also polarized. Polarized SM radiation turns out to be very sensitive to the orientation of the axes of the magnetic and electric fields, which cause hyperfine splitting of nuclear levels. This sensitivity makes it possible to determine the structure of hyperfine interaction fields in handling crystals or to obtain data on the texture in powder samples. In addition, the polarization of SM radiation enables the use of polarization analysis when reflecting SM radiation from nuclear resonance samples with an antiferromagnetic structure obtaining spectra of radiation reflected by resonant nuclei in absence of interference with nonresonant scattering channels [55, 56].

4. On the capabilities of sources of synchrotron Mössbauer radiation

The above-listed features of synchrotron Mössbauer radiation offer options for its unique applications. In this section, we describe experimental studies in which these properties, each individually and in their totality, made it possible to obtain previously inaccessible physical results.

4.1 Ultrathin magnetic layers

4.1.1 Magnetism of multilayer mirrors. When studying multilayer systems, all the advantages of SM radiation are used without exception. Since experiments with multilayer mirrors deal with coherent scattering in the geometry of total external reflection, such studies require high radiation directivity. To determine magnetic ordering in cases where it occurs in multilayer mirrors, polarization of the radiation is necessary. The intensity and resonance characteristics of the radiation make it possible to better isolate nuclear resonance scattering in systems containing iron.

A remarkable confirmation of this option is study [57], in which the structure of magnetization in a multilayer ^{57}Fe/Cr mirror was examined. In this system, the iron layers are separated by a chromium spacer, the thickness of which determines the type of exchange interaction between adjacent iron layers. Depending on the thickness of the chromium layers, this interaction can be both a ferromagnetic and an antiferromagnetic type. However, there is a transition region of chromium spacer thicknesses, where the type of exchange interaction between the iron layers is not strictly defined. The authors explored just this kind of multilayer system to obtain amazing results that were not previously predicted in theoretical models.

The measurements were carried out under conditions of grazing incidence of rays on a layered mirror. The obtained angular dependences of the reflection of rays from the mirror are presented in Fig. 10. When measuring the dependence presented by curve *1* in Fig. 10, the main part of the intensity of the incident beam was nonresonant radiation. Under such conditions, the reflection from the mirror was formed primarily due to electron scattering. When measuring the dependence displayed by curve *2*, the beam was purely resonant. Therefore, both scattering channels in the system under study, nuclear and electronic, were involved in the process. Curve *1* shows that the reflection intensity saturates below the critical angle and smoothly decreases above this angle, making characteristic oscillations due to the interference of the radiation scattered from the upper and lower boundaries of the layered system. At an angle slightly above 19 mrad, a maximum is observed due to Bragg diffraction on the layered periodic structure of the mirror. Fitting the electronic reflectivity curve yielded a structure period of 2.24 nm with a chromium layer thickness of 1.58 nm and an iron layer thickness of 0.66 nm. It is this structure of the layered system that met the intermediate conditions for the implementation of ferromagnetic or antiferromagnetic exchange interaction between ultrathin layers of iron.

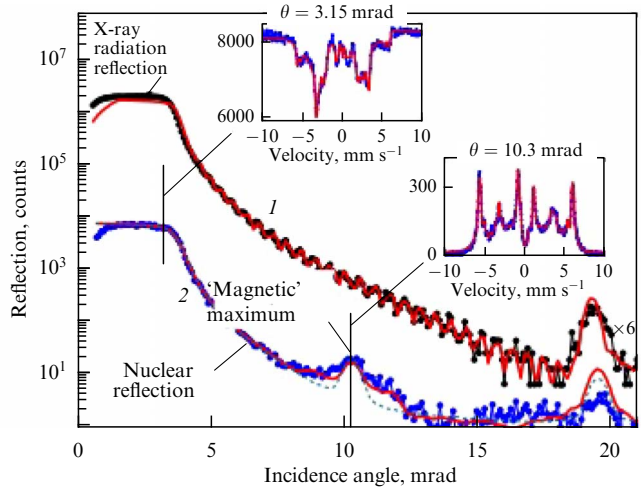

Figure 10. Angular dependences of electronic (upper curve *1*) and mixed electron-nuclear (lower curve *2*) reflection of synchrotron radiation from a multilayer mirror $[^{57}Fe/Cr]_{30}$ under conditions of grazing incidence in critical angle region at a temperature of 4 K in the absence of an external magnetic field. Insets show Mössbauer spectra near critical angle of total reflection and at the position of the magnetic nuclear Bragg maximum. Solid red lines represent theoretical fits to experimental data. Green dotted curve represents theoretical dependence for the model of antiferromagnetic ordering of hyperfine fields in iron layers (from [57]).

Curve *2* was obtained in the following way. First of all, the Mössbauer spectrum was measured at each angular position of the mirror. The spectrum changed with the variation in the angle. While near the critical angle, this was an absorption spectrum; at a grazing angle of $\theta = 10.3$ mrad, it was transformed into a scattering spectrum. The reflection intensity was calculated by integrating over the spectrum energy obtained at a given angle. Based on the totality of all measurements, the final angular dependence was plotted. A significant feature of the electron-nuclear reflection curve was the appearance of an additional maximum at an angle of ~ 10 mrad. In this way, nuclear Bragg diffraction, associated with magnetic order in the system, manifested itself. The emergence of a maximum indicates the existence of antiferromagnetic ordering of neighboring iron layers. As for the intensity of the magnetic peak, it exhibited a dependence on the magnetic field applied to the mirror, which was directed in the mirror plane perpendicular to the scattering plane. The magnetic peak reached its maximum value in a field of 0.15 T and vanished in a field of 1 T. With a change in the field strength, the shape of the Mössbauer spectrum at the angular position of the reflection maximum underwent a significant transformation. The ratio of the intensities of hyperfine magnetic splitting lines corresponding to nuclear transitions with magnetic quantum numbers $M = \pm 1$ and $M = 0$ indicated the existence of a mixed ferromagnetic and antiferromagnetic ordering of fields in the system of iron layers.

A comprehensive analysis of all the data obtained revealed an amazing picture, presented in Fig. 11. A very unusual behavior of magnetization vectors in iron layers with increasing depth was discovered. In the neighboring iron layers on the surface of the mirror, in the absence of an external field, an almost antiferromagnetic ordering of the magnetic moments of the iron layers was observed. When the depth from the surface of the mirror increases, the magnetic moments of the iron layers rotate, forming a helical structure. In a system of even layers, rotation occurs in one direction, while in a system of odd layers, it happens in the opposite direction. The rotation of magnetic moments in opposite directions leads, at a depth of just above 20 nm, to their almost ferromagnetic alignment in the odd and even layers of iron. Next, magnetic moments in each subsystem abruptly

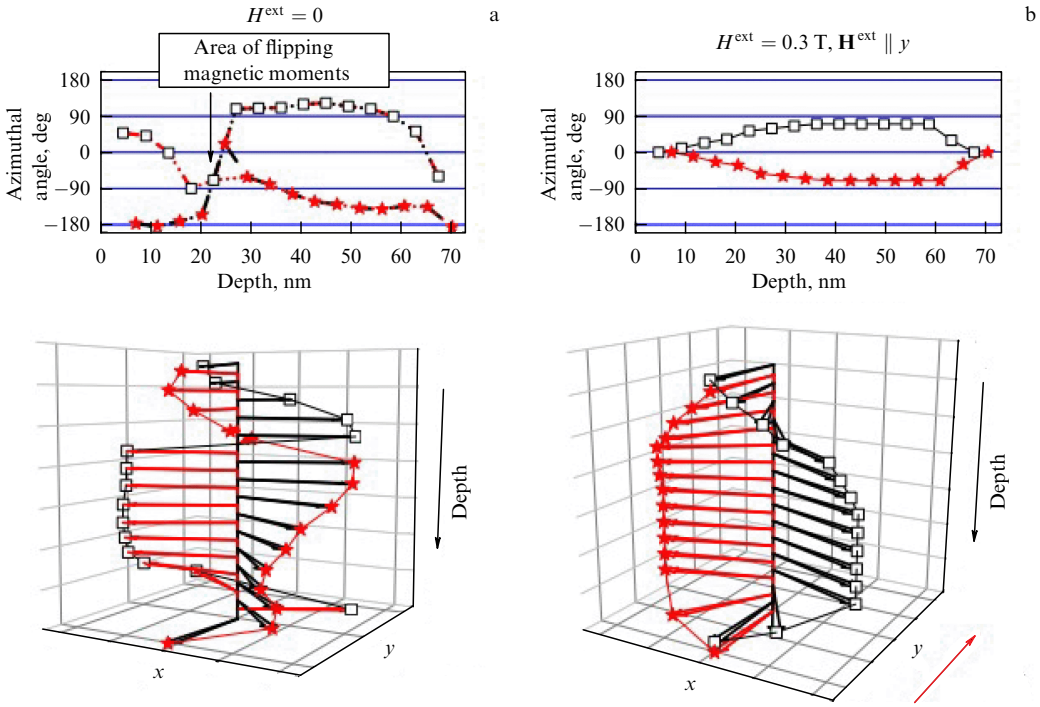

Figure 11. Mutual orientation of hyperfine magnetic fields in iron layers at various depths from mirror surface: (a) in the absence of an external magnetic field and (b) after applying an external field of 0.3 T directed perpendicular to the scattering plane. Stars indicate fields in even layers of iron, and rectangles, in odd layers (from [57]).

flip, as is clearly visible in Fig. 11a. With a further increase in depth, the magnetic moments rotate in directions opposite to the previous ones, but again towards each other.

After applying an external field, the structure and behavior of the magnetization of the iron layers look completely different (Fig. 11b). Ferromagnetic ordering is observed on the surface of the mirror and at a depth of ~ 70 nm. With the increase in depth, magnetic moments in adjacent iron layers rotate in opposite directions, and at a depth of ~ 45 nm, their almost pure antiferromagnetic ordering is realized.

The results obtained in the study under consideration showed that, by varying the thickness of ultrathin magnetic layers, it is possible to widely modify the properties of devices based on multilayer magnetic systems. The source of synchrotron Mössbauer radiation provided unique opportunities to examine microscopic amounts of matter under extreme conditions in terms of temperature and external magnetic field. Mössbauer reflectance spectra measured at various grazing angles showed a particularly high sensitivity to the distribution of magnetization in multilayer systems from the surface layer to depth, which demonstrates a clear advantage of the nuclear resonance reflectometry method over alternative techniques, for example, polarization neutron reflectometry.

4.1.2 Magnetic molecules. The remarkable capabilities of synchrotron Mössbauer radiation offered new options to study the properties of magnets in the form of single molecules. Molecular magnets represent an attractive class of nanomagnetic objects that can be applied in molecular spintronics and quantum computers. In the experiment under consideration [58], the subject of study was magnetic molecules of tetrairon (III) (Fe_4), which have a propeller-like molecular structure. The properties of the molecule are determined by a combination of high molecular spin and the existence in the molecule of a double-well energy potential that counteracts magnetization reversal. The question was whether the magnetic bistability of the molecule would persist after being deposited on a bearing surface. The surface of a flat polycrystalline gold substrate was used to deposit magnetic molecules. Figure 12a shows an image of the molecule after its chemical absorption on the surface of a substrate. A monolayer of such molecules was prepared in which the enrichment with the resonance isotope was 95%. The ESRF source of SM radiation was used for the studies. Figure 12b shows the experimental setup.

A directed beam of resonant radiation emitted by an $^{57}FeBO_3$ crystal was focused onto a target down to a micron size in diameter. Such dimensions made it possible to operate in a grazing incidence geometry, which made it possible to increase the effective thickness of the target and achieve the necessary sensitivity in studying a molecular monolayer. Mössbauer spectra of hyperfine splitting of iron nucleus levels in tetrairon molecules were recorded by collecting radiation reflected by the surface of the substrate. In such a geometry, the beam penetrated a layer of molecules, and absorption spectra were recorded. The effective target thickness in the experimental geometry contains the coefficient $2/(\sin q)$, where q is the grazing angle between the sample surface and the direction of the incident radiation. For the conditions under consideration, the grazing angle was 0.1°, which provided a 1100-fold increase in the thickness of the target. Mössbauer spectra were measured at various temperatures in the range of 2.2–40 K and 2.2–11 K using a superconducting helium-exchange gas cryomagnetic system. No external magnetic field was applied.

Due to the high brightness of the SM source, an unprecedentedly detailed picture of the interaction between a molecule and a surface was obtained, revealing the structural, electronic, and magnetic properties of adsorbed molecular magnets. The Mössbauer spectra of tetrairon molecules are displayed in Fig. 13. The spectrum measured at the lowest temperature, 2.2 K, contains six lines that indicate hyperfine magnetic splitting of nuclear levels. The main conclusion that follows from this observation is that, at low temperatures, molecules attached to the surface can remain magnetic, and the magnetic bistability of molecules on the surface can persist. Such conclusions are the answer to the main questions posed in the work. A slight broadening of the spectral lines indicates the presence of spin fluctuations that are slow compared to the time of collision of the quantum with the nucleus. The progressive collapse of the spectrum with the formation of a single central line indicates that the characteristic times of fluctuations decreases with increasing temperature.

Due to the exceptional sensitivity of synchrotron Mössbauer spectroscopy, it has also been demonstrated that molecules on the surface undergo structural deformations that were previously undetectable by X-ray absorption and scanning probe microscopy techniques.

4.1.3 Magnetic Friedel oscillations. It is well known that exchange interaction results in a spatial correlation of electron spins, in particular, in the emergence of spontaneous magnetization of materials. Since the number of neighbors on the surface of a magnetic material is less than that in a bulk, the exchange interaction on the surface can create a polarization of electron spins different from those in the bulk, and, consequently, a different magnetization. Based on this observation, it can be expected that the magnetization should change when moving from the surface of the magnet

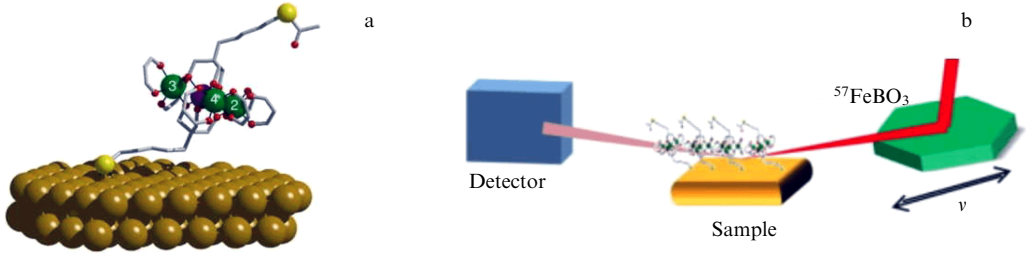

Figure 12. (a) Single magnetic tetrairon molecule chemically adsorbed on the surface of gold. (b) Grazing incidence of synchrotron Mössbauer radiation on a monolayer of magnetic molecules (from [58]).

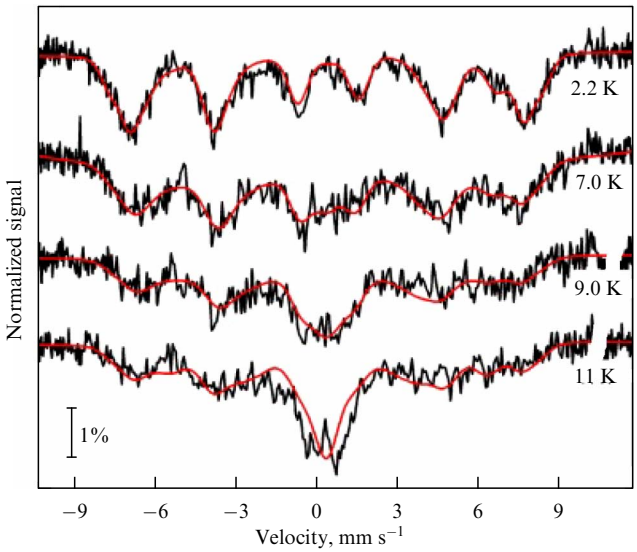

Figure 13. Evolution of Mössbauer spectra of a monolayer of single magnetic tetrairon molecules with increasing temperature (from [58]).

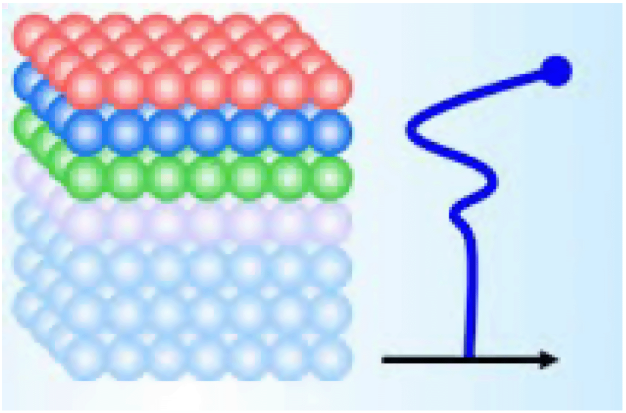

Figure 14. Scheme of magnetization setting up when moving from the surface of a magnetic sample into its depth: Friedel magnetic oscillations (from [60]).

into its volume. For example, almost 50 years ago, the French physicist Friedel predicted that the magnetization in the surface layer of iron should change with depth in the form of oscillations. According to Friedel, such oscillations should represent periodic spatial changes in atomic-scale magnetization. Later theoretical studies showed that, in an iron crystal, on the surface of which the (001) planes extend, layer-by-layer oscillations of magnetization should occur in moving from the surface of the crystal to the bulk [59]. Friedel magnetic oscillations are shown schematically in Fig. 14. Oscillations, as can be seen, should quickly decay, approaching the value characteristic of the volume of the crystal [60].

Observing such oscillations is an extremely challenging problem. One of the conceivable options is associated with probing magnetism using the ^{57}Fe isotope. This approach is based on the hyperfine splitting of ^{57}Fe nucleus levels being very sensitive to the presence of a local magnetic field. To implement this approach, a magnetism-sensitive layer of a resonant isotope should be embedded into a matrix of a nonresonant one. Hyperfine splitting of the energy levels of isotope nuclei could be detected using Mössbauer spectroscopy with registration of conversion electrons. The hyperfine interaction parameters extracted from the Mössbauer spectra of the embedded layer would make it possible to make conclusions regarding the change in magnetization upon passing from the surface of the crystal to its depth with atomic-scale spatial resolution. In addition, the values of isomer shifts and quadrupole interaction extracted from the spectra would provide information about changes in the s-electron density and the electric field gradient on nuclei moving deeper from the surface. However, the use of a radionuclide Mössbauer source in an experiment of this kind would be completely ineffective. Obtainment of the required measurement accuracy would require a huge amount of time, on the scale of several weeks, during which it would be impossible to avoid covering the surface of the sample with residual gas in the vacuum chamber where the sample is to be placed.

The authors of the study under consideration [61] used another method only accessible when using an SM radiation source. The high directivity of the radiation made it possible to carry out with high angular resolution an experiment on the total external reflection of radiation from the surface of a sample, while the high radiation intensity made it possible to reduce the measurement time by several orders of magnitude.

Iron films were prepared by the epitaxial method. To deposit layers of iron atoms, a substrate of magnesium oxide MgO, which has a cubic crystal lattice, was used. The (001) face extended onto the surface of the plate with dimensions of $10 \times 10 \times 0.5$ mm^3. Iron isotopes were successively deposited onto the substrate, forming a crystalline film of Fe(001). The total thickness of the deposited iron layer was 5 nm. It mainly consisted of the ^{56}Fe isotope; however, the body of this layer contained at a certain depth an atomic layer of ^{57}Fe 0.1 nm thick. After a single sample was prepared in the epitaxy chamber, it was immediately moved to the measurement chamber. An ultra-high vacuum of about $10^{-8}-10^{-9}$ Pa was maintained in the sample preparation and measurement chambers, and the sample temperature was 300 K. A polarized beam of SM radiation was incident on the sample at a grazing angle of 0.1° and underwent total external reflection, as shown in Fig. 15a. The energy of the incident radiation was scanned in the region of gamma resonance in ^{57}Fe nuclei.

Since the iron layer was magnetized along the beam direction, the magnetic polarization vector of the radiation made an angle of 90° to the field on the nuclei. In this geometry, only $M = \pm 1$ transitions could be excited. Under such excitation conditions, the Mössbauer spectrum contained only four lines. The absorption spectra obtained for four samples with different depths of the resonance layer are shown in Fig. 15b. To the right of them, the corresponding arrangement of ^{57}Fe layers performing as resonant probes is schematically shown. Due to the high brightness of the SM source, the measurement time for each spectrum was only a few hours.

The spectra obtained made it possible to determine the parameters of hyperfine splitting of nuclear levels and the values of local magnetic fields. Using the theoretical relation between hyperfine fields and magnetization, the main result was obtained — a layer-by-layer variation in magnetization at the surface of the iron film. Friedel's magnetic oscillations were observed for the first time. On the surface of the film, the magnetization turned out to be maximum; then, the amplitude of the magnetization oscillations quickly decreased. The

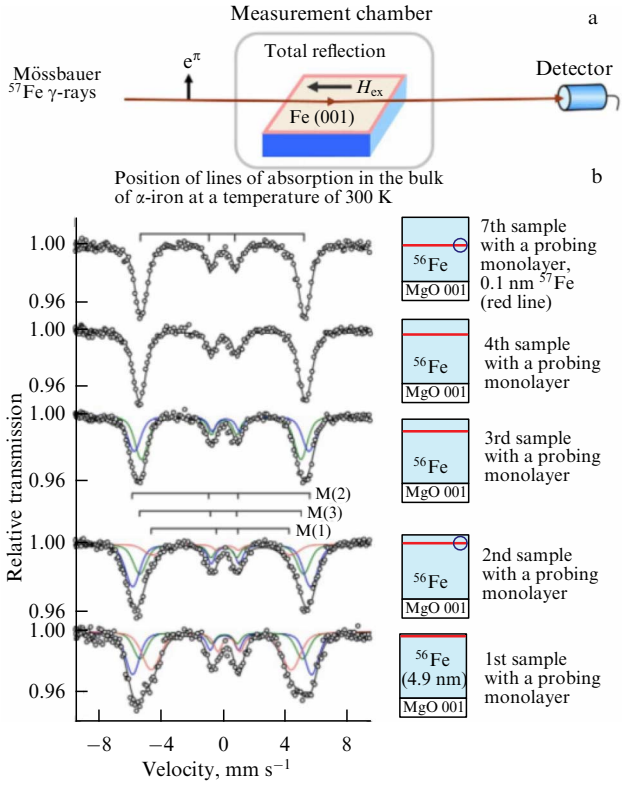

Figure 15. (a) Experimental setup, (b) Mössbauer spectra of resonant ^{57}Fe layers located at various depths in a nonresonant matrix (from [61]).

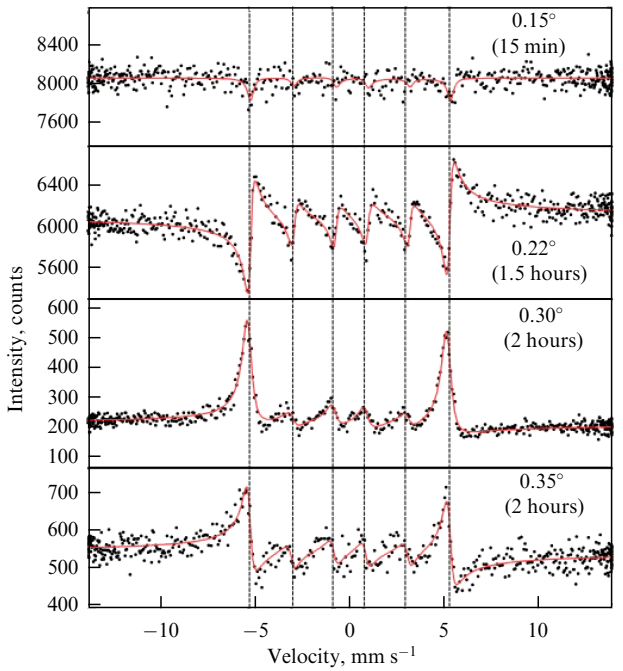

Figure 16. Mössbauer reflection spectra in the geometry of a grazing beam at various grazing angles. Vertical lines indicate positions of nuclear resonances. Red lines represent theoretical calculations (from [62]).

oscillations decayed completely after the fourth atomic layer. Thus, the magnetic oscillations predicted by Friedel almost 50 years ago were finally observed. One can hope that the method demonstrated in the experiment will become an effective tool for studying spintronics devices.

4.1.4 Reflection from a thin ^{56}Fe film with a built-in ^{57}Fe monolayer. Quantum interference of Mössbauer γ-rays. Among many interesting applications of artificial multilayer systems, of special interest is the possibility of realizing in them the conditions of giant magnetoresistance. The phenomenon of giant magnetoresistance is an important consequence of the dependence of the probability of electron scattering in a ferromagnet on the direction of electron spins. In multilayer systems, it is manifested through a significant variation in electrical resistance when the relative direction of magnetization of adjacent layers alters. Systems with giant magnetoresistance are already widely used in spintronics devices, for example, in highly sensitive magnetic field sensors, which are used to read information in hard drives, biosensors, etc. To enhance the performance of such systems, information about the state of magnetization at a certain depth near the interface is required. Only a few techniques make it possible to directly determine the electronic and magnetic states of a multilayer system near a buried interface. In particular, Mössbauer spectroscopy can provide the necessary information due to its high sensitivity to the hyperfine interaction between electrons and nuclei.

As it concerns ultrathin films, the most effective technique to study them is the total external reflection of Mössbauer radiation. However, laboratory radionuclide radiation sources cannot be used in this case due to their relatively weak luminosity. Japanese physicists successfully conducted an experiment unique in its sophistication with an ultra-thin layer by using a source of SM radiation, the brightness of which exceeded that of the radionuclide source (^{57}Co 100 mCurie) by 100,000 times [62]. SM radiation was used to study nuclear gamma resonance spectra in a 14-nm-thick Cr/Fe/Cr film on an MgO substrate. A monolayer of ^{57}Fe was introduced into the film at a depth of 6 nm. Mössbauer reflection spectra from the film, measured at various grazing angles, are shown in Fig. 16. The spectra obtained contain a great deal of important information. First of all, the observed hyperfine structure of the spectra makes it possible to extract the required information about the splitting of the levels of the ^{57}Fe nucleus, between which a transition is observed, and, based on this information, make a conclusion regarding the electric and magnetic fields at the interface of a buried monolayer. As for the resonance lines in the obtained spectra, the variety of their shapes is simply amazing, but the most important point is that it contains very rich information. The spectral lines are in this case nothing more than Fano resonances formed in the scattering process under study due to interference between the potential electronic and resonant nuclear scattering channels. The interference conditions are determined by a number of experimental parameters, including the angle of incidence of radiation on the film and the depth of the nuclear resonance monolayer.

Near the angular region of total external reflection, the incident radiation barely reaches the resonant layer located at a depth of 6 nm. As a result, in the spectrum corresponding to a grazing angle of 0.15°, interaction with nuclei is observed very faintly in the form of absorption lines. However, an increase in the grazing angle by a mere 0.07° is sufficient for the nuclei to enter the irradiation zone and for a pronounced interference of the electronic and nuclear scattering channels to be observed, which is manifested in a clearly cut dispersion shape of the resonance lines.

Dispersive contrast arises due to a change in the phase of the nuclear scattering amplitude by π radians when passing through resonance. As for the phase of the electron scattering amplitude, it does not change in a given energy interval. When scattering by nuclei and electrons occurs in the same phase, the amplitudes are added; otherwise, they are subtracted. These cases are respectively referred to as constructive and destructive interference. The sign of asymmetry indicates the relationship between the phases of electron and nuclear scattering at different sides of the resonance, which determines the shape of the interference pattern. In the spectrum at a grazing angle of 0.22°, the dispersion contrast is most pronounced: interference is destructive on the left side of the resonance, when the radiation energy is less than the resonant value, and constructive on the other side of the resonance. The large depth of contrast indicates that the amplitudes of electron and nuclear scattering are approximately equal.

At the next angular position, the interference pattern changes radically. Here, the dispersion contrast is much weaker. The nuclear scattering channel becomes dominant. However, at a grazing angle of 0.35°, the contrast of the interference pattern is enhanced again, but the sign of the asymmetry of the dispersion lines turns out to be opposite to that at a grazing angle of 0.22°. The asymmetry of the resonance lines depends, among other things, on the phase acquired by radiation on the path from the film surface to the interface of the $^{56}Fe/^{57}Fe$ layers. At a fixed depth of the ^{57}Fe layer, this phase is determined by the grazing angle of the radiation when incident on the film. For example, at a grazing angle of 0.22°, this phase is close to $\pi/2$ radians, while at a grazing angle of 0.35°, it is close to $3\pi/2$. This explains the inversion of the dispersion contrast with the considered change in grazing angles.

Summarizing, the authors of the experiment described above, first, showed that magnetization near the boundaries of buried functional films can be determined and, second, proposed a method for direct measurement of the radiation phase at such boundaries using the interference of electron and nuclear resonant scattering.

4.2 Extreme temperature and pressure conditions. Earth's magnetism

Earth holds many secrets. One of the intriguing questions is the nature of the magnetism of Earth's interior, including Earth's crust, mantle, and core. Earth's magnetic field is primarily generated by its internal structure. Thus, according to the generally accepted hypothesis, the field is created essentially due to the circulation of an electrically conductive fluid in the outer core at a depth of approximately 3000 to 5000 km below Earth's surface. However, Earth's crust near the surface can also contribute to the magnetic field, in those areas where ferromagnetic minerals are contained. For example, iron oxide in the form of hematite, α-Fe_2O_3, being a weak ferromagnetic material, is abundant in both continental and oceanic-crust rocks.

As for Earth's mantle, it was believed for a long time that it does not take part in the formation of the geomagnetic field, since ferromagnetic minerals would lose their magnetic properties when colliding blocks of Earth's crust subduct, the lower blocks immersing in the hot mantle. At the high temperatures, 1000 K and higher, existing in the mantle, the magnetic properties of ferromagnetic materials are destroyed. For example, the temperature above which hematite magnetism vanishes is 948 K at atmospheric pressure. The issue of temperatures of magnetic phase transitions at high pressures inherent in the mantle matter remained open until recently. Only some information obtained using satellites and aeromagnetic survey data on the residual magnetism of rock fragments captured by magma during volcanic eruptions was available. This data indicated that sources of deep magnetic anomalies can exist, but the nature of these sources remained unknown. There were only guesses about the magnetism associated with iron oxides.

Recently, an international research team at ESRF successfully reconstructed mantle pressure and temperature in the laboratory and used SM radiation to study the magnetic properties of polymorphic varieties of iron oxide Fe_2O_3 under the extreme conditions of the mantle [63].

A powder of artificially synthesized iron oxide in the form of hematite α-Fe_2O_3 was placed in microscopic quantities between the diamond anvils of a pressure cell heated from two sides by laser beams (Fig. 17a). A focused beam of SM radiation was passed through the sample. To study the magnetic state of the latter, Mössbauer absorption spectra were measured. The pressure in the sample chamber could vary in the range from atmospheric to 90 GPa (the latter corresponds to depths of approximately 2000 km), and the temperature could be elevated from room temperature to 1300 K.

The behavior of the magnetic properties of α-Fe_2O_3 under such conditions was not known before. The experiments in which pressure and temperature were varied revealed transitions of hematite into other polymorphic states of iron oxide, in particular, the formation of known polymorphic states such as h-Fe_2O_3, q-Fe_2O_3, i-Fe_2O_3, and z-Fe_2O_3, and, in addition, previously unknown iron oxide was also discovered.

Due to the unique properties of SM radiation, Mössbauer spectra were measured with excellent resolution up to the highest temperatures and pressures achievable under experimental conditions, which made it possible to obtain rich information on the evolution of the parameters of hyperfine splitting of spectra in a wide range of pressures and temperatures. Figure 17b shows changes in the magnetic hyperfine splitting of the hematite spectrum with increasing temperature at various pressures on the sample: atmospheric, 19.4 GPa, and 25.4 GPa.

The main result is that the collapse of the spectrum, i.e., the disappearance of magnetic ordering in hematite, shifts significantly towards high temperatures with increasing pressure. It is amazing that, at a pressure of 25.4 GPa, the critical temperature was already approaching 1200 K. The result obtained shows that hematite in the lithospheric plates subducting into the mantle can still retain its magnetic properties. Presumably, it is the only magnetic phase in the process of the plunging of lithospheric plates into the mantle to a depth of 300 to 600 km. Thus, it may be concluded that the mantle can be magnetically active.

Another interesting result is noteworthy. The authors compared the location of the linear magnetic anomaly, which on a map of Earth stretches along the western rim of the Pacific Ocean, with the distribution of lithospheric plates subducting into the mantle in this area to discover an astounding correlation. Previously, these anomalies were associated with the history of magnetic field reversal and were considered traces of the trajectory of Earth's magnetic pole during the reversal process. Now, the results obtained suggest an alternative interpretation of the nature of such an anomaly. According to the authors, it is most likely

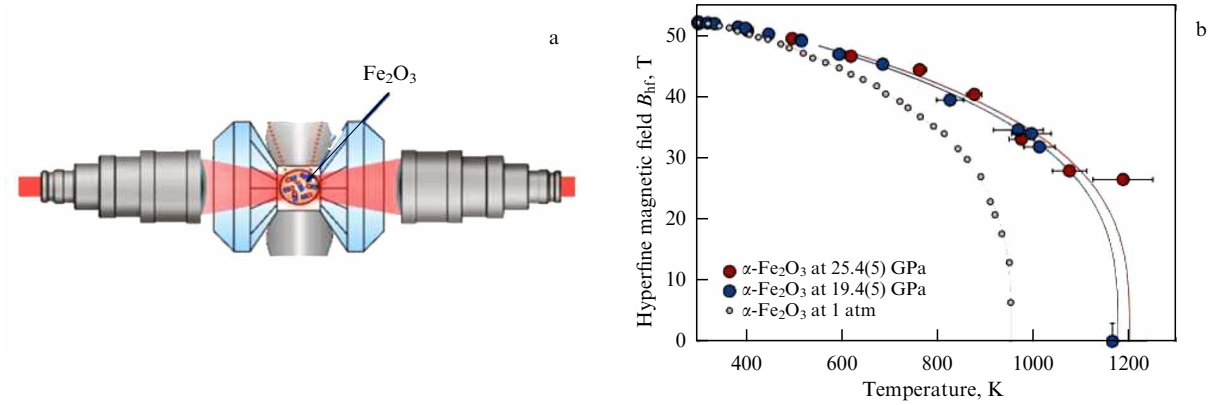

Figure 17. (a) Schematic view of a pressure cell with diamond anvils (image created by Timofey Fedotenko). (b) Temperature dependences of the hyperfine magnetic field in hematite at various pressures (from [63]).

associated with lithospheric plates subducting into the mantle, located in the region under consideration at depths of up to 300–600 km.

4.3 Quasi-elastic Rayleigh scattering

The high energy resolution typical of Mössbauer spectroscopy can be successfully used to study quasi-elastic scattering. Such processes are characterized by extremely small changes in the energy of scattered radiation, caused by the slow dynamics of atoms. In using Mössbauer beams, the sensitivity to energy changes is particularly high. To identify variations in energy on the scale of the width of the nuclear level, an energy analysis of the scattered radiation spectra should be carried out using a Mössbauer filter. Study [64] was the first to apply a Mössbauer filter to analyze scattered radiation. In this way, nuclear resonance scattering was observed, during which the nuclear spin rotated. The authors of [65] used a similar approach to observe and study nuclear magnetic resonance in the excited state of ^{57}Fe nuclei. Quasi-elastic scattering associated with ultrasonic excitation of a nuclear target was observed in [66–70]. In all the mentioned studies, a radionuclide source of Mössbauer radiation was used. The options for using a synchrotron Mössbauer source in studies of quasi-elastic scattering were demonstrated in [71]. However, significant progress in this area has only been achieved by Japanese physicists in recent years [72]. In addition to the source with a line width $\Delta E \approx 15$ neV, intended for the analysis of scattered radiation with high resolution, a Mössbauer source with a line width $\Delta E \approx 15$ μeV was developed. These sources are referred to below as narrowband and broadband, respectively. To create the latter source, the method proposed in [73] was used. Enormous line broadening was achieved by exciting high-frequency oscillations of the crystal lattice along the surface of the emitting crystal. Lattice oscillations, which were generated by applying a radio frequency field to the crystal, were due to magnetoelastic coupling between iron atoms. The crystal was maintained at room temperature. High-frequency oscillations of the crystal lattice caused a broadening of the hyperfine structure lines, which were maximally spaced from each other at room temperature, resulting in the formation of a radiation spectrum with a width of up to 200 natural widths of the nuclear level. Some applications of a synchrotron Mössbauer source with a variable emission linewidth have been studied by Japanese physicists. We only provide an example in which quasi-elastic scattering of radiation on a glycerol sample was studied in a wide temperature range, up to its transition to the liquid phase.

The upper spectra in Fig. 18a, b represent instrumental functions. In Fig. 18a, this is the Mössbauer absorption spectrum in stainless steel, obtained using a narrow-band source, and, in Fig. 18b, the absorption spectrum in a standard black absorber obtained using a broadband source. Panels (a) and (b) below show Mössbauer absorption spectra in the same absorbers, but this time incident on them was the radiation scattered on a sample of glycerol, which was maintained at various temperatures somewhat differing from the melting point in its immediate vicinity, $T_m \approx 290$ K. All spectra with a narrow-band source were measured up to the melting point.

A broadening of the spectral line was clearly observed, indicating an increase in quasi-elastic scattering in glycerol with increasing temperature. However, it is clearly seen that, before reaching the melting point, the spectrum of quasi-elastic scattering already begins to go beyond the energy region of observation. Therefore, with a further increase in temperature, a more suitable broadband SM source was used. With this source, the authors were able to reliably observe nuclear resonance scattering from glycerol even in the liquid phase, almost 10 K above the melting point, and determine the width of the quasi-elastic scattering spectrum. An important methodological expansion of the properties of a synchrotron Mössbauer source offers new options for its application, namely, it enables studying slow atomic and molecular dynamics in the condensed state of matter, including glassy structures, polymers, biological materials, and liquid crystals.

4.4 Aliens from outer space bringing secrets of interplanetary space to Earth

The study of meteorites — aliens from interplanetary space — provides insight into the distant past of the solar system and makes it possible to reconstruct the history of the origin of the planets. Meteorites, first of all, carry the secrets of the origin and formation of planet-like objects, such as asteroids. Many studies are devoted to the examination of meteorites also because it sheds light on the state of Earth's interior, inaccessible to modern science, and enables identification of the geochemical patterns of the evolution of their matter.

The authors of [74], which we consider in this section, studied a rare representative of the meteorite family, pallasite.

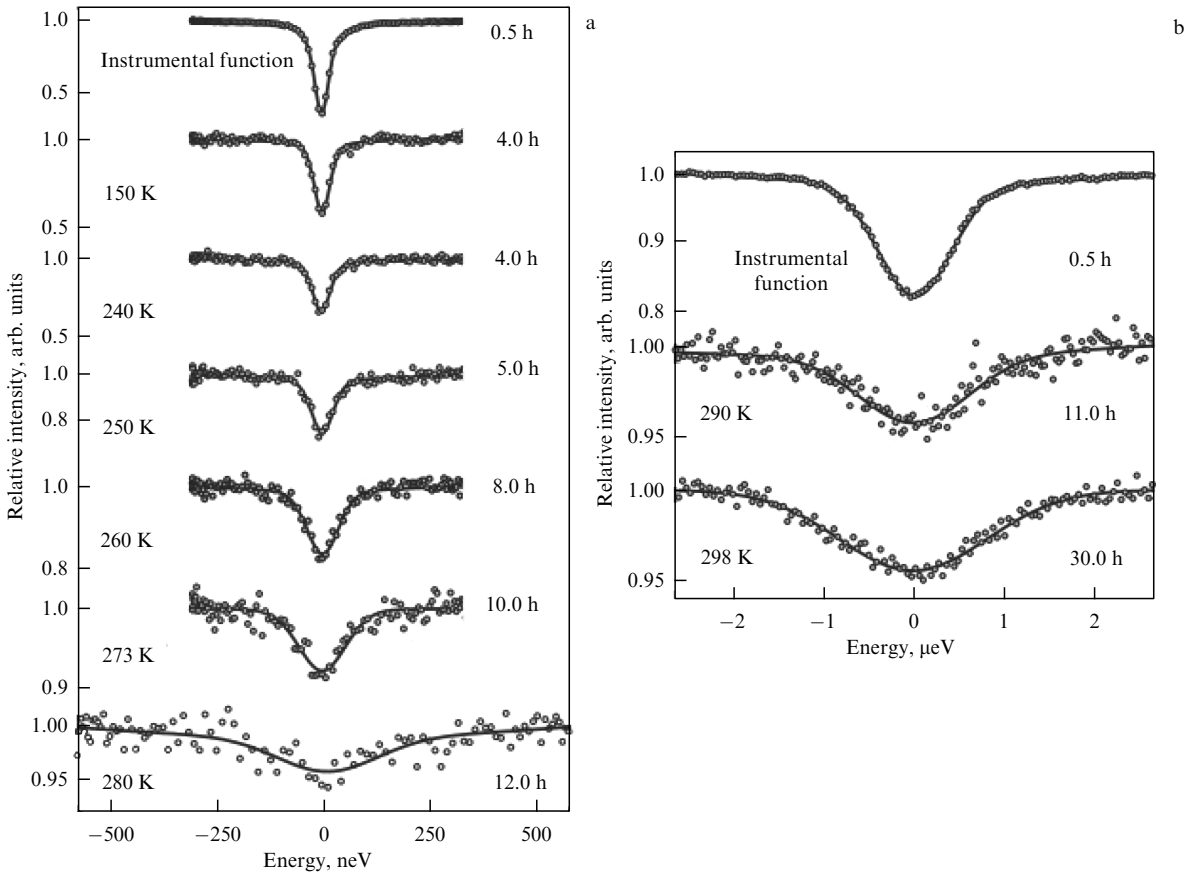

Figure 18. Spectra representing quasi-elastic scattering of synchrotron Mössbauer radiation by glycerol at various temperatures: (a) narrow-band SM radiation and (b) broadband SM radiation (from [72]).

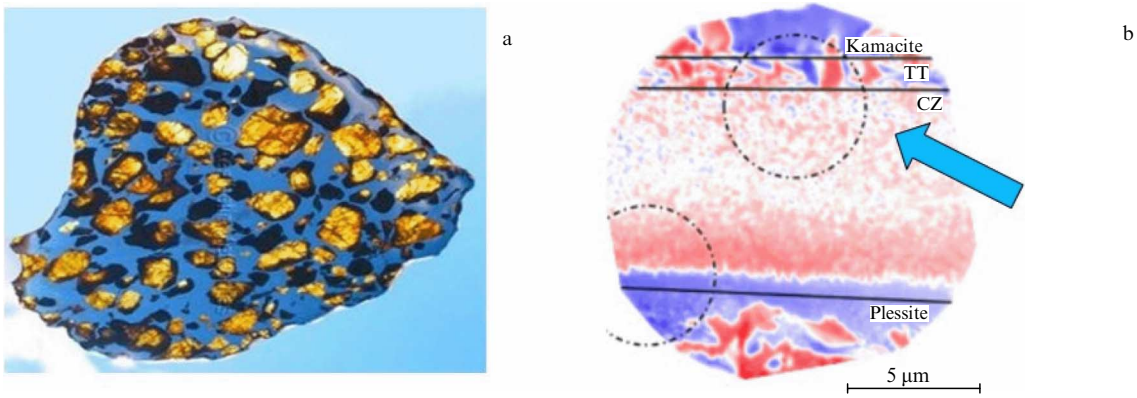

Figure 19. (a) Polished plate of pallasite, a stony-iron meteorite. (b) Image of the magnetization of a small area in the zone of the iron-nickel alloy, obtained by X-ray photoemission microscopy (from [75]).

It is a stony-iron meteorite, consisting of olivine crystals in an iron-nickel matrix. Figure 19a shows a transparent polished section of pallasite. The mosaic contrast between the metal alloy and the olivine windows is very picturesque.

The pallasites that arose in the asteroid's mantle cooled very slowly, at a rate of 5 K every million years. Therefore, metal microstructures 'frozen' in these meteorites can reveal a time pattern of the development of the geological history of their ancestors. They also contain the primordial history of magnetism, which arose millions of years ago due to the dynamics of planetary matter. The development of such processes in time, a temporal memory about them, could be recorded in the so-called cloud zones of iron and nickel alloys, arising as a result of their spinodal decay. The cloud zone is a transition region between the phases of the iron-nickel alloy. It contains microinclusions of metal phases of various structures, such as kamacite α-Fe(Ni) (body-centered phase of the alloy), taenite γ-Fe(Ni) (face-centered phase of the alloy), tetrataenite (ordered γ-phase of FeNi), plessite, which is a mixture of α-Fe(Ni) + γ-Fe(Ni), etc. Using X-ray photoemission microscopy, it was possible to reveal the structure of magnetic domains in various zones of the Fe–Ni alloy [75] (Fig. 19b).

Mössbauer spectroscopy makes it possible to determine quantitative characteristics of magnetism. In [74], a source of SM radiation was used to study microinclusions of an Fe–Ni alloy in the above-mentioned cloud zone of pallasite with high spatial resolution.

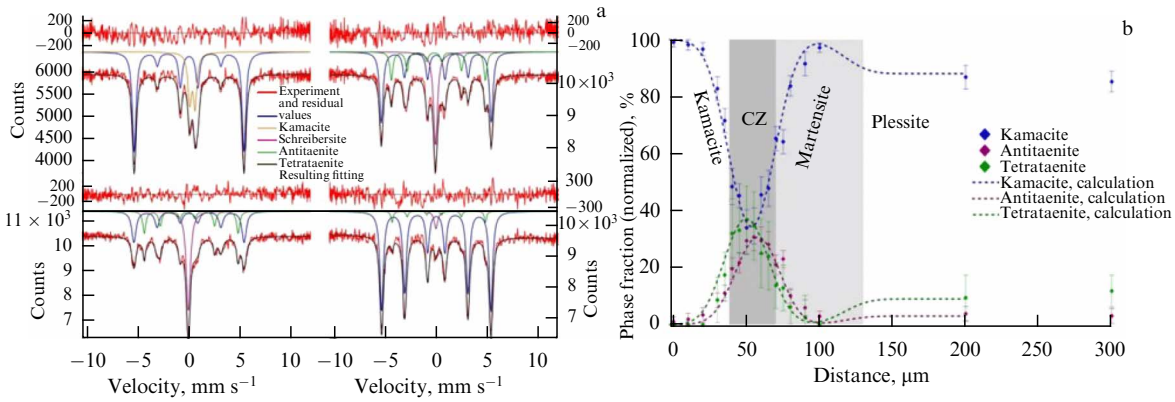

Figure 20. (a) Two representative Mössbauer spectra of a plessite sample: on the left — in the cloud zone, and on the right — in the plessite zone. (b) An example of the phase distribution of an iron-nickel alloy centered in the cloud zone (CZ), obtained from a set of Mössbauer spectra [74].

Inasmuch as SM radiation can be localized with high accuracy in various parts of the cloud zone, the Mössbauer spectra of microparticles of various phases of the iron-nickel alloy can be measured in these areas. The spectra were recorded in steps of 5–10 μm. Due to the high radiation intensity, the authors were able to obtain a spectrum at each point within one hour with a fairly high statistical accuracy. The precision measurements made it possible to monitor changes in phase inclusions in the main microstructural formations (Fig. 20) and determine the parameters of the hyperfine structure of such inclusions.

The results obtained posed new fundamental questions related to the emergence of remanent magnetization in the cloud zone of iron-nickel meteorites. Further experimental studies are required to reveal the properties of their magnetization. It should be noted that the method used exhibited the remarkable capabilities of Mössbauer spectroscopy based on using an SM source. In the near future, the ESRF will launch a Mössbauer nanoscope with a spatial resolution of 200–600 nm.

5. Concluding remarks

A remarkable feature of the Mössbauer effect is that gamma radiation emitted by a bound nucleus can retain and maintain the property of coherence of intranuclear currents. In elastic nuclear resonant scattering, the absorption and emission of a quantum cannot be considered to be two independent scattering events, and this is true even when the lifetime of the isomeric state is enormous on nuclear scales. In this case, nuclear resonance fluorescence is a single-quantum process in which the scattered radiation is coherent with the incident radiation.

The concept of delocalized nuclear excitation — nuclear exciton — makes it possible to reveal the collective nature of the process of elastic scattering of a single gamma quantum by an ensemble of nuclei in a crystal. Coherent fluorescence of a nuclear ensemble should be considered a macroscopic quantum mechanical phenomenon. The crystal operates like a kind of macroscopic quantum resonator.

Coherent nuclear fluorescence governs the entire picture of the interaction of gamma radiation with the nuclear ensemble. Parameters characteristic of resonant interaction with an individual nucleus, such as linewidth, lifetime, and the ratio of the probabilities of elastic and inelastic scattering, undergo radical changes. In particular, under conditions of coherent nuclear fluorescence, a significant enhancement of the radiative scattering channel occurs. This enhancement in its most striking form is observed in Bragg nuclear diffraction.

Diffraction from the nuclear lattice of a crystal without the admixture of electron scattering, pure nuclear diffraction, was discovered in 1969 [34]. Purely nuclear diffraction of gamma radiation features a very complex interference nature. The well-known interference of X-ray radiation in geometric three-dimensional space is complemented by interference in energy and spin spaces.

Pure nuclear diffraction in an iron borate crystal [41] made it possible to generate coherent Mössbauer radiation from ^{57}Fe in modern synchrotrons in the absence of a potentially huge background of electron scattering. The first experimental source of synchrotron Mössbauer radiation from ^{57}Fe nuclei was created at the European Synchrotron Radiation Facility (ESRF) in 1997 [51]. A modernized source was built in 2007 at the SPring8 accelerator center [53]. Currently, these centers operate upgraded sources on an ongoing basis [53, 54].

An SM radiation source has a number of important advantages over a radionuclide source. The first feature is that the SM radiation spectrum contains no recoilless component. Due to the absence of a nonresonant background, the depth of the resonance lines in the absorption spectra, what we call the resonance effect, increases significantly. This circumstance makes it possible to study samples containing a poor amount of the resonant isotope. No less important, it enables a significant ($\sim 10^3$ times) reduction in the measurement time with conventional samples while providing the same accuracy of spectrum parameters. The high directionality of SM radiation is effectively used in coherent scattering processes [62, 76]. Since the synchrotron radiation exciting the nuclei is almost completely linearly polarized, the radiation emitted by the nuclei is also polarized. Polarized SM radiation turns out to be very sensitive to the orientation of the axes of the magnetic and electric fields, which cause hyperfine splitting of nuclear levels. This sensitivity allows the structure of hyperfine interaction fields to be determined when working with crystals or data on the texture in powder samples to be obtained. In addition, the polarization of SM radiation makes it possible to use polarization analysis when reflecting SM radiation from nuclear resonance samples with an antiferromagnetic structure and to obtain spectra of radiation reflected by resonant nuclei in absence interference with nonresonant scattering channels.

The unique properties of synchrotron Mössbauer radiation make it possible to conduct previously unfeasible physical experiments and obtain valuable scientific results. The range of options is very wide. It includes a variety of research in condensed matter physics, quantum optics, geophysics, planetary science, and other areas of science. Examples include the discovery of such an amazing phenomenon as Friedel magnetic oscillations [61], which were theoretically predicted almost 50 years ago; discovery of an unusual helical structure of magnetization in a regular multilayer system [57]; identification and study of the magnetic bi-stability of single molecules deposited on a substrate [58] (nanomagnets of this kind can be used in molecular spintronics and quantum computers); and measurement of magnetization at the boundaries of buried functional films [62], which can operate as elements of highly sensitive magnetic field sensors.

One of the most important applications of SM sources is exploration of matter under extreme conditions of pressure, temperature, and magnetic field [63, 77]. For these purposes, pressure cells with diamond anvils, ultra-low and ultra-high temperatures with laser heating, and ultra-strong magnetic fields are used. Due to the high concentration of the radiation beam in space, nanoscopic studies are feasible [74]. The capabilities of SM radiation are far from being exhausted. One can confidently assert that its future is great.

Acknowledgments. The author is deeply grateful to the International Mössbauer Committee, which awarded him the IBAME Science Award "in recognition of his pioneering theoretical development and experimental implementation of nuclear γ-ray optics and his seminal contribution to the development of the Synchrotron Mössbauer Source."

References

1. Mössbauer R L, in *The Rudolf Mössbauer Story: His Scientific Work and Its Impact on Science and History* (Eds M Kalvius, P Kienle) (Berlin: Springer, 2012) p. 3, https://doi.org/10.1007/978-3-642-17952-5_1; Mössbauer R L, in *The Rudolf Mössbauer Story: His Scientific Work and Its Impact on Science and History* (Eds M Kalvius, P Kienle) (Berlin: Springer, 2012) p. 37, https://doi.org/10.1007/978-3-642-17952-5_3
2. Heitler W *The Quantum Theory of Radiation* 3rd ed. (Oxford: Oxford Univ. Press, 1954)
3. Black P J, Moon P B *Nature* **188** 481 (1960)
4. Wigner E P *Phys. Rev.* **98** 145 (1955)
5. Smirnov G V, Shvyd'ko Yu V *Sov. Phys. JETP* **68** 444 (1989); *Zh. Eksp. Teor. Fiz.* **95** 777 (1989)
6. Bernstein S, Campbell E C *Phys. Rev.* **132** 1625 (1963)
7. Black P J, Duerdoth I P *Proc. Phys. Soc.* **84** 169 (1964)
8. Trammell G T, in *Chemical Effects of Nuclear Transformations* (Proc. Intern. Atomic Energy Agency, Vol. 1) (Vienna: IAEA, 1961) p. 75
9. Afanas'ev A M, Kagan Yu *JETP Lett.* **2** 81 (1965); *Pis'ma Zh. Eksp. Teor. Fiz.* **2** 130 (1965)
10. Zaretskii D F, Lomonosov V V *Sov. Phys. JETP* **21** 243 (1965); *Zh. Eksp. Teor. Fiz.* **48** 368 (1965)
11. Haas M et al. *Phys. Status Solidi B* **149** 283 (1988)
12. Shvyd'ko Yu V, Smirnov G V *J. Phys. Condens. Matter* **1** 10563 (1989)
13. Smirnov G V *Hyperfine Interact.* **123/124** 31 (1999)
14. Smirnov G V et al. *Phys. Rev. A* **71** 023804 (2005)
15. Smirnov G V et al. *Phys. Rev. A* **76** 043811 (2007)
16. Haas M *Phys. Lett. A* **361** 391 (2007)
17. Smirnov G V *Hyperfine Interact.* **27** 203 (1986); Van Bürck U *Hyperfine Interact.* **27** 219 (1986)
18. Smirnov G V *Hyperfine Interact.* **97/98** 551 (1996)
19. Smirnov G V *Izv. Ross. Akad. Nauk. Ser. Fiz.* **67** 984 (2003); Smirnov G V, in *The Rudolf Mössbauer Story: His Scientific Work and Its Impact on Science and History* (Eds M Kalvius, P Kienle) (Berlin: Springer, 2012) p. 317, https://doi.org/10.1007/978-3-642-17952-5_16
20. Gerdau E, de Waard H (Eds) "Nuclear resonant scattering of synchrotron radiation" *Hyperfine Interactions* **123/124** (1999/2000)
21. Rüffer R, Chumakov A I "Historical developments and future perspectives in nuclear resonance scattering," in *Modern Mössbauer Spectroscopy. New Challenges Based on Cutting-Edge Techniques* (Topics in Applied Physics, Vol. 137, Eds Y Yoshida, G Langouche) (Singapore: Springer, 2021) p. 1
22. Röhlsberger R, Evers J "Quantum optical phenomena in nuclear resonant scattering," in *Modern Mössbauer Spectroscopy. New Challenges Based on Cutting-Edge Techniques* (Topics in Applied Physics, Vol. 137, Eds Y Yoshida, G Langouche) (Singapore: Springer, 2021) p. 105
23. Ewald P P *Rev. Mod. Phys.* **37** 46 (1965); *Usp. Fiz. Nauk* **89** 287 (1966)
24. von Laue M *Röntgenstrahl-Interferenzen* (Frankfurt: Akademische Verlag, 1960)
25. Battermann B W, Cole H *Rev. Mod. Phys.* **36** 681 (1964)
26. Kagan Yu *Hyperfine Interact.* **123/124** 83 (1999)
27. Hannon J P, Trammell G T *Hyperfine Interact.* **123/124** 127 (1999)
28. Afanas'ev A M, Kagan Yu *Sov. Phys. JETP* **21** 215 (1965); *Zh. Eksp. Teor. Fiz.* **48** 327 (1965)
29. Kagan Yu, Afanas'ev A M, Perstnev I P *Sov. Phys. JETP* **27** 819 (1968); *Zh. Eksp. Teor. Fiz.* **54** 1530 (1968)
30. Smirnov G V, Chumakov A I *Phys. Rev. A* **100** 043830 (2019)
31. Voitovetskii V K et al. *Sov. Phys. JETP* **27** 729 (1968); *Zh. Eksp. Teor. Fiz.* **54** 1361 (1968)
32. Artem'ev A N et al. *JETP Lett.* **15** 226 (1972); *Pis'ma Zh. Eksp. Teor. Fiz.* **15** 320 (1972)
33. Artem'ev A N et al. *Sov. Phys. JETP* **37** 136 (1973); *Zh. Eksp. Teor. Fiz.* **64** 261 (1973)
34. Smirnov G V et al. *JETP Lett.* **9** 70 (1969); *Pis'ma Zh. Eksp. Teor. Fiz.* **9** 123 (1969)
35. Belyakov V A, Aivazyan Yu M *JETP Lett.* **7** 368 (1968); *Pis'ma Zh. Eksp. Teor. Fiz.* **7** 477 (1968)
36. Belyakov V A, Aivazyan Yu M *JETP Lett.* **9** 393 (1969); *Pis'ma Zh. Eksp. Teor. Fiz.* **9** 637 (1969)
37. Mirzababaev R M et al. *Phys. Lett. A* **37** 441 (1971)
38. Mirzababaev R M, Sklyarevskii V V, Smirnov G V *Phys. Lett. A* **41** 349 (1972)
39. Smirnov G V et al. *Sov. Phys. JETP* **51** 603 (1980); *Zh. Eksp. Teor. Fiz.* **78** 1196 (1980)
40. Zelepukhin V et al. *Vopr. Atom. Nauki Tekh.* (4(33)) 76 (1985)
41. Smirnov G V et al. *JETP Lett.* **43** 352 (1986); *Pis'ma Zh. Eksp. Teor. Fiz.* **43** 274 (1986)
42. Stepanov E P et al. *Sov. Phys. JETP* **39** 562 (1974); *Zh. Eksp. Teor. Fiz.* **66** 1150 (1974)
43. Smirnov G V *Hyperfine Interact.* **125** 91 (2000)
44. Smirnov G V *J. Exp. Theor. Phys.* **133** 7 (2021); *Zh. Eksp. Teor. Fiz.* **160** 13 (2021)
45. Smirnov G V et al. *Phys. Rev. A* **84** 053851 (2011)
46. Afanas'ev A M, Kagan Yu *Sov. Phys. JETP* **37** 987 (1973); *Zh. Eksp. Teor. Fiz.* **64** 1958 (1973)
47. Hannon J P, Trammell G T *Phys. Rev.* **169** 315 (1968)
48. Hannon J P, Trammell G T *Phys. Rev.* **186** 306 (1969)
49. Hannon J P, Carron N J, Trammell G T *Phys. Rev. B* **9** 2791 (1974)
50. Smirnov G V *J. Exp. Theor. Phys.* **135** 137 (2022); *Zh. Eksp. Teor. Fiz.* **162** 165 (2022)
51. Smirnov G V et al. *Phys. Rev. B* **55** 5811 (1997)
52. Pankhurst Q A et al. *J. Non-Cryst. Solids* **287** 81 (2001)
53. Mitsui T et al. *J. Synchrotron Rad.* **16** 723 (2009)
54. Potapkin V et al. *J. Synchrotron Rad.* **19** 559 (2012)
55. Baulin R A et al. *Surf. Interfaces* **27** 101521 (2021)
56. Baulin R A et al. *JETP Lett.* **113** 162 (2021); *Pis'ma Zh. Eksp. Teor. Fiz.* **113** 175 (2021)
57. Andreeva M A et al. *Phys. Rev. B* **97** 024417 (2018)
58. Cini A et al. *Nat. Commun.* **9** 480 (2018)
59. Wang C S, Freeman A J *Phys. Rev. B* **24** 4364 (1981)
60. Schirber M *Physics* **13** 156 (2020)
61. Mitsui T et al. *Phys. Rev. Lett.* **125** 236806 (2020)
62. Fujiwara K et al. *J. Phys. Soc. Jpn.* **90** 084705 (2021)

63. Kupenko I et al. *Nature* **570** 102 (2019)
64. Artem'ev A N, Smirnov G V, Stepanov E P *Sov. Phys. JETP* **27** 547 (1968); *Zh. Eksp. Teor. Fiz.* **54** 1028 (1968)
65. Heinman N D et al. *Phys. Rev.* **184** 281 (1969)
66. Asher J, Cranshaw T E, O'Connor D A *J. Phys. A* **7** 410 (1974)
67. Tsankov L T *J. Phys. A* **14** 275 (1981)
68. Popov S L, Smirnov G V, Shvyd'ko Yu V *JETP Lett.* **49** 747 (1989); *Pis'ma Zh. Eksp. Teor. Fiz.* **49** 651 (1989)
69. Popov S L, Smirnov G V, Shvyd'ko Yu V *Hyperfine Interact.* **58** 2463 (1990)
70. Shvyd'ko Yu V, Smirnov G V *J. Phys. Condens. Matter* **4** 2663 (1992)
71. Masuda R et al. *Jpn. J. Appl. Phys.* **47** 8087 (2008)
72. Mitsui T et al. *J. Phys. Soc. Jpn.* **91** 064001 (2022)
73. Shvyd'ko Yu V et al. *Europhys. Lett.* **19** 723 (1992)
74. Blukis R et al. *Meteorit. Planet. Sci.* **52** 925 (2017)
75. Bryson J F J et al. *Earth Planet. Sci. Lett.* **396** 125 (2014)
76. Andreeva M A et al. *Phys. Met. Metallogr.* **91** (Suppl. 1) 22 (2001)
77. Gavrilyuk A G et al. *JETP Lett.* **117** 126 (2023); *Pis'ma Zh. Eksp. Teor. Fiz.* **117** 132 (2023)